

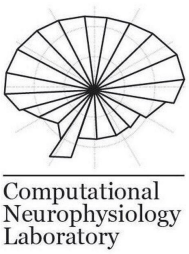


**UNIVERSIDADE FEDERAL DO RIO GRANDE DO NORTE**

**INSTITUTO DO CÉREBRO**

**PROGRAMA DE PÓS-GRADUAÇÃO EM NEUROCIÊNCIAS**

**LABORATÓRIO DE NEUROFISIOLOGIA COMPUTACIONAL**

**JOSÉ HENRIQUE TARGINO DIAS GOIS**

# NEURONAL CORRELATES OF LOCOMOTION SPEED IN THE DORSAL CA1 OF THE RAT HIPPOCAMPUS: NEW INSIGHTS ON THE SPEED CELLS

CORRELATOS NEURONAIS DA VELOCIDADE DE LOCOMOÇÃO EM CA1 DORSAL DO HIPOCAMPO DE RATOS: NOVAS ANALISES NAS CÉLULAS DE VELOCIDADE

**NATAL**

**2020**

JOSÉ HENRIQUE TARGINO DIAS GOIS

# NEURONAL CORRELATES OF LOCOMOTION SPEED IN THE DORSAL CA1 OF THE RAT HIPPOCAMPUS: NEW INSIGHTS ON THE SPEED CELLS

CORRELATOS NEURONAIS DA VELOCIDADE DE LOCOMOÇÃO EM CA1 DORSAL DO HIPOCAMPO DE RATOS: NOVAS ANALISES NAS CÉLULAS DE VELOCIDADE

Tese apresentada ao curso de Pós-graduação em Neurociências, da Universidade Federal do Rio Grande do Norte, como requisito parcial à obtenção do título de Doutor em Neurociências (área de concentração: neurocomputação, neuroengenharia e neuroterapia).

Orientador: Prof. Dr. Adriano Bretanha Lopes Tort

NATAL

2020

Universidade Federal do Rio Grande do Norte - UFRN
Sistema de Bibliotecas - SISBI
Catalogação de Publicação na Fonte. UFRN - Biblioteca Setorial Árvore do Conhecimento - Instituto do Cérebro - ICE

Gois, José Henrique Targino Dias.
Neuronal correlates of locomotion speed in the dorsal CA1 of the rat hippocampus: new insights on the speed cells = Correlatos neuronais da velocidade de locomoção em CA1 dorsal do hipocampo de ratos: novas analises nas células de velocidade / José Henrique Targino Dias Gois. - Natal, 2020.
60f.: il.

Tese (Doutorado em Neurociências) - Instituto do Cérebro, Universidade Federal do Rio Grande do Norte, 2020.
Orientador: Adriano Bretanha Lopes Tort.

1. Spatial navigation. 2. Rats - Locomotion speed. 3. Hippocampus. 4. Neurons. 5. Electrophysiology. I. Tort, Adriano Bretanha Lopes. II. Título.

RN/UF/BSICe CDU 612.822

Elaborado por ISMAEL SOARES PEREIRA - CRB-15/741

JOSÉ HENRIQUE TARGINO DIAS GOIS

# NEURONAL CORRELATES ON THE LOCOMOTION SPEED IN THE DORSAL CA1 OF THE RAT HIPPOCAMPUS: NEW INSIGHTS ON THE SPEED CELLS

Tese apresentada ao curso de Pós-graduação em Neurociências, da Universidade Federal do Rio Grande do Norte, como requisito parcial à obtenção do título de Doutor em Neurociências (área de concentração: neurocomputação, neuroengenharia e neuroterapia).

Aprovada em: 06/12/2019

BANCA EXAMINADORA

Prof. Dr. Adriano Bretanha Lopes Tort
Orientador(a)
Universidade Federal do Rio Grande do Norte

Prof. Dr. Daniel Yasumasa Takahashi
Membro interno
Universidade Federal do Rio Grande do Norte

Prof. Dr. Rodrigo Roncy Pereira
Membro interno
Universidade Federal do Rio Grande do Norte

Prof. Dr. Werner Treptow
Membro externo
Universidade de Brasília

Prof. Dr. Wilfredo Blanco Figuerola
Membro externo
Universidade Estadual do Rio Grande do Norte

Aos leitores.

To the readers

## AKNOWLEDGMENT

I thank the Buzsáki laboratory for making data publicly available at http://crcns.org/, a data-sharing website supported by NSF and NIH, USA. I also thank Kiah Hardcastle, Niru Maheswaranathan, and the Giocomo laboratory for making LN-model codes publicly available at https://github.com/GiocomoLab/. I thank Adriano Bretanha Lopes Tort not only for advisement, but also being a multidimentional companion through scientific initiation. I thank Brazil citizens for the taxes, which aided research and survivability through this scientific initiation. I thanks those who have collaborated through this path, adding insights and challenges towards maturity in many aspects. I thanks those I cannot name but have been part of contributing on their own way, even without me noticing.

## FINANCIAL SUPPORT

Supported by Conselho Nacional de Desenvolvimento Científico e Tecnologico (CNPq) and Coordenação de Aprerfeiçoamento de Pessoal de Nível Superior (CAPES).

## AGRADECIMENTOS

Eu agradeço ao laboratório de Buzsáki por tornar público os dados disoníveis no http://crcns.org/, um portal de compartilhamento de dados financiado por NSF e o NIH nos EUA. Eu também agradeço a Kiah Hardcastle, Niru Maheshwaranathan e ao laboratório de Giocomo por disponibilizar os códigos do modelo Linear-Não-Linear pubplicados em https://github.com/GiocomoLab/. Eu agradeço Adriano Bretanha Lopes Tort não somente pela orientação, mas pela companhia multidimencional na iniciação científica. Eu agradeço aos cidadões brasileiros pelos impostos pagos que suportaram a pesquisa e as despesas através dessa iniciação científica (2009-2019). Eu agradeço aos diversos colaboradrores que adicionaram ideias e desafios em direção a maturidade em diversos aspectos. Eu agradeço àqueles que eu não sou capaz de nomear mas contribuiram de sua própria maneira, mesmo sem eu poder notar.

## SUPORTE FINANCEIRO

Financiado pelo Conselho Nacional de Desenvolvimento Científico e Tecnologico (CNPq) e pela Coordenação de Aprerfeiçoamento de Pessoal de Nível Superior (CAPES).

## ABSTRACT

Edward Tolman postulated the existence of cognitive maps in the brain to explain the animal capability of spatial navigation. Since then, neuroscience seeks to describe brain components underlying this capability. In the present work, we describe advancements in the characterization of a neural sub-population engaged in coding the scalar velocity of rat locomotion. Upon analyzing an open database, we re-discovered the existence of a velocity correlation present in the rate of emission of action potentials of neurons in the dorsal hippocampus. we found that this correlation is independent of theta oscillation frequency (4-12 Hz) and stable over space and time; moreover, it also persists in different arenas. We then classified the neurons as excitatory and inhibitory by the action potential waveform shapes, the rate of emission of action potentials, and the temporal inter-dependency of action potential emission between pairs of neurons. This classification revealed that, by using Pearson's r coefficient (speed score) as a correlation metric, in the square open-field arena, only inhibitory neurons high-correlated with locomotion speed (henceforth, speed), even though there was a modulation of the average of the excitatory neurons. Intriguingly, when checking speed correlates in the linear arena, speed score made indistinguishable the correlation among neuronal classes. We then formulated the hypothesis that the apparent locomotion speed correlation of pyramidal neurons in the linear arena is spurious, due to a by-product of their spatial code. To prove this, we simulated artificial neurons that emitted action potentials influenced by the actual animal behavior; the simulated neurons coded either speed or space. The simulation replicated real data Pearson's r coefficient classifications – true positives in the square arena and false positives in the linear arena for those cells encoding speed. To solve this ethological interdependency, we adopted a new metric of speed correlation – the ratio of the difference of linear-non-linear models prediction accuracy based on speed and position over the prediction accuracy of the two-variable model. This analysis disentangled the ethological issue, satisfactorily classifying the simulated neurons and confirming the spurious hypothesis correlates, and the prevalence of speed correlates in interneurons. The results of the present work demonstrated that a genuine speed correlation is present in the dorsal CA1 of the hippocampus of rats in inhibitory neurons.



Keywords: spatial navigation, locomotion speed, rats, hippocampus, neurons, electrophysiology

## RESUMO

Edward Tolman postulou a existência de mapas cognitivos no cérebro para explicar a capacidade animal de navegar pelo espaço. Desde então, neurocientistas buscam descrever componentes cerebrais que suportam essa capacidade. No presente trabalho, descrevemos avanços na caracterização de uma sub-população neural que participa na representação da velocidade escalar na locomoção de ratos. Através da análise de um banco de dados aberto, nós re-descobrimos a existência do correlato de velocidade na taxa de emissão de potenciais de ação de neurônios da região CA1 do hipocampo dorsal de ratos. Essa correlação é independente da frequência da oscilação de theta (4-12 Hz) e é estável através do espaço e tempo; além disso, essa correlação persiste em diferentes arenas. A classificação de neurônios entre prováveis excitatórios ou inibitórios revelou que, ao utilizar o coeficiente r de Pearson (índice de velocidade) como métrica de representação de velocidade nos neurônios, somente neurônios inibitórios apresentaram-se como altamente correlacionados com a velocidade na arena quadrada, embora os neurônios excitatórios apresentem uma modulação na média da taxa de emissão de potenciais de ação. Intrigantemente, na arena linear a mesma métrica tornou indistinguiveis as classificações neurais pela correlação com a velocidade. Então, formulamos a hipótese que a aparente correlação com a velocidade dos neurônios excitatórios na arena linear é espúria – um subproduto da correlação de velocidade com o espaço. Para testar essa hipótese, simulei neurônios artificiais que emitem potenciais de ação influenciados pelo comportamento locomotor do animal; essas simulações codificam velocidade ou espaço. As simulações replicaram a classificação pelo índice de velocidade encontrados nos dados reais – ou seja, código de posição não correlaciona com velocidade na arena quadrada mas sim na arena linear. Para solucionar essa interdependência etológica, nós adotamos uma nova métrica de correlação com a velocidade: a razão da diferença da acurácia de predição dos modelos linear-não-linear baseados em velocidade e posição sobre a acurácia de predição do modelo das duas variáveis. Essa análise resolveu o problema etológico, classificou satisfatoriamente as simulações e confirmou a hipótese da correlação espúria na arena linear e a prevalencia da correlação nos neurônios inibitórios. Os resultados deste trabalho demonstra uma correlação genuina da velocidade de locomoção nos neurônios inibitórios na área CA1 do hipocampo dorsal de ratos.



Keywords: navegação espacial, velocidade, ratos, cérebro, hippocampo, neurônios, eletrofisiologia

## FIGURE INDEX

## LISTA DE ABREVIATURAS

| | |
|---|---|
| **C** | Center (of the arena) |
| **CA1** | Cornus ammonis 1 |
| **CCG** | Cross-correlogram |
| **CRCNS** | Collaborative research in computational neuroscience |
| **E** | Edge (of the arena) |
| **FR** | Firing rate |
| **Int** | Interneuron |
| **LFP** | Local field potential |
| **LLHi** | Log-likelihood increase |
| **LN** | Linear-non-linear-Poisson |
| **OLM** | Oriens-lacunosum moleculare |
| **Pyr** | Pyramidal |
| **Q** | Quadrant ($1^{st}$, $2^{nd}$, $3^{rd}$ and $4^{th}$) |
| **RMS** | Root mean square |
| **SD** | Standard deviation |
| **SEM** | Standard error of the mean |
| **SPC** | Spikes per theta cycle |
| **W** | Whole (arena) |

**SUMMARY**

# PREAMBLE

Spatial navigation relies on visual landmarks as well as on self-motion information. In familiar environments, both place and grid cells maintain their firing fields in darkness, suggesting that they continuously receive information about locomotion speed required for path integration. Consistently, “speed cells” have been previously identified in the hippocampal formation and characterized in detail in the medial entorhinal cortex. Here we performed a thorough investigation of speed-correlated firing in the hippocampus. We show that CA1 has speed cells that are stable across contexts, position in space and time. Moreover, their speed-correlated firing occurs within theta cycles, independently of theta frequency. Interestingly, a physiological classification of cell types reveals that all CA1 speed cells are inhibitory. In fact, while speed modulates pyramidal cell activity, only the firing rate of interneurons can accurately predict locomotion speed on a sub-second time scale. These findings shed new light on network models of navigation.

The results presented in this thesis were published in the article *“Characterizing Speed Cells in the Rat Hippocampus”,* by ZHTD Góis and ABL Tort, Cell Reports 2018; 25(7):1872-1884.e4. doi: 10.1016/j.celrep.2018.10.054. Updates of this thesis can be found at **https://www.gois.wiki.br/thesis**.

# 1 INTRODUCTION

## 1.1. NAVIGATION SYSTEMS

The ability to navigate across space is crucial for the survival of several species. To that end, the brain must be able to construct representations of past, present and future locations, and continuously compute information about the self and the environment (FERBINTEANU; SHAPIRO, 2003; DRAGOI; BUZSÁKI, 2006; BUCKNER, 2010; BUZSÁKI; MOSER, 2013; SANDERS et al., 2015). Current theories on spatial navigation assert that the brain uses two mechanisms for spatial coding: one conveying sensory inputs from environment landmarks (allocentric navigation), and another based on path integration or "dead reckoning" (O'KEEFE, 1976; MCNAUGHTON et al., 1996; WHISHAW; BROOKS, 1999; BUZSÁKI; MOSER, 2013). The latter does not depend on external stimuli but on integrating information about previous location, movement direction, and locomotion speed (egocentric navigation) (WHISHAW, 1998; BUZSÁKI, 2005; MCNAUGHTON et al., 2006).

## 1.2. NEURAL CORRELATES OF SPATIAL NAVIGATION

During the last decades, several neuronal correlates of spatial navigation have been discovered and localized to specific brain regions (MOSER; KROPFF; MOSER, 2008; GRIEVES; JEFFERY, 2017). Among them, the best-known examples are the place cells in the hippocampus (O'KEEFE; DOSTROVSKY, 1971) and the grid cells in the medial entorhinal cortex (HAFTING et al., 2005). Given their periodically repeating pattern of spatial firing, grid cells have been suggested to take part in path integration (HAFTING et al., 2005; FUHS; TOURETZKY, 2006; MCNAUGHTON et al., 2006). Consistent with this, neurons correlated with locomotion speed (henceforth, speed) have been previously found in the medial entorhinal cortex (SARGOLINI, 2006; WILLS; BARRY; CACUCCI, 2012) and recently studied in more detail (KROPFF et al., 2015; HINMAN et al., 2016; YE et al., 2018). Place cells, on the other hand, would signal allocentric spatial relationshis, and the primary drive for their place-selective firing would stem from sensory information such as visual landmarks (O'KEEFE; DOSTROVSKY, 1971; O'KEEFE; SPEAKMAN, 1987)(O'KEEFE; CONWAY, 1978; O'KEEFE; SPEAKMAN, 1987). Evidence for this comes with changes in the orientation of spatial cues (O'KEEFE; CONWAY, 1978; MULLER; KUBIE, 1987; SHARP; KUBIE; MULLER, 1990). Nevertheless, place cells also exhibit place-selective

action potentials in darkness when animals explore familiar environments (MCNAUGHTON; LEONARD; CHEN, 1989; QUIRK; MULLER; KUBIE, 1990), suggesting that they are also capable of keep track of animal position using self-motion information (MCNAUGHTON et al., 1996; KNIERIM; KUDRIMOTI; MCNAUGHTON, 1998).

## 1.3. HIPPOCAMPUS AND SPATIAL NAVIGATION

Adjacent structures of the hippocampal formation and the medial septum are likely to convey the hippocampus with information about head direction and speed (TAUBE; MULLER; RANCK, 1990; LEVER et al., 2003; HAFTING et al., 2005; MCNAUGHTON et al., 2006; FUHRMANN et al., 2015; YE et al., 2018). Similar to the medial entorhinal cortex (SARGOLINI, 2006; WILLS; BARRY; CACUCCI, 2012), hippocampal neurons have also been shown to exhibit skipikg activity correlated with speed (MCNAUGHTON; BARNES; O'KEEFE, 1983; WIENER; PAUL; EICHENBAUM, 1989; O'KEEFE et al., 1998; ZHANG et al., 1998; CZURKÓ et al., 1999, 2011; HIRASE et al., 1999; EKSTROM et al., 2001; NITZ; MCNAUGHTON, 2004; MAURER et al., 2005). These previous studies, however, typically reported average neuronal firing rate as a function of speed and did not consider whether hippocampal neurons would code for speed on a sort time scale, nor did they investigate the robustness of hippocampal speed correlates across time, space and contexts. Of note, though mostly focused on entorhinal cortex neurons, the study of (KROPFF et al., 2015) has also reported speed cells with similar characteristics in the hippocampus.

## 1.4. NEURONAL CORRELATES OF LOCOMOTION SPEED

Given the renewed interest in speed coding in the entorhinal-hippocampal network (KROPFF et al., 2015; HINMAN et al., 2016; YE et al., 2018), in the present work we sought to perform a through characterization of speed-correlated firing in the hippocampus. Our results confirm and expand previous reports by showing that (1) speed cells exist in the dorsal CA1, that (2) speed coding by firing rate of CA1 neurons is stable across space, elapsed time, and contexts, that (3) CA1 speed coding occurs within theta cycles, and that (4) CA1 speed cells exclusively comprise interneurons. While the latter finding contrasts with previous reports showing speed-correlated firing of hippocampal pyramidal cells (e.g., (MCNAUGHTON; BARNES; O'KEEFE, 1983; WIENER; PAUL; EICHENBAUM, 1989; CZURKÓ et al., 1999; HIRASE et al., 1999; EKSTROM et al., 2001; MAURER et al., 2005), here we demonstrate that, in open fields, such correlations are only apparent when averaging firing rate values over fixed speed bins, but not on the finer time scale of animal behavior.

Consistently, (5) only the firing rate of interneurons, but not of pyramidal cells, accurately predicts speed in the open field on a sub-second time scale. Moreover, we further show that (6) although pyramidal cells exhibit speed-correlated action potentials in a linear track task, such correlations can be explained by spatial coding along with the interdependence of space and speed due to the nature of the task (i.e., animals stereotypically run fastest in the middle of the linear track and slowest on the edges). Such correlations reveal that Pearson's r coefficient is not an appropriated metric to evaluate speed influence in neuronal activity; to prove this (7) we utilized recorded real locomotion to simulate speed or space encoding neurons. These simulations ratified the unappropriated usage of Pearson's r coefficient to measure speed influence in neuronal action potentials. (8) Therefore, we utilized a linear-non-linear model (HARDCASTLE et al., 2017) that use both speed and space influence to estimate firing rate; then, we utilized the Pearson's squared r coefficient ($r^2$) between the real and estimated firing rate as fitting accuracy. (9) Finally, we propose a substitute metric of speed score – the difference of prediction accuracy from linear-non-linear models of speed and position single variable over the prediction accuracy of same model with both variables; this metric overcame false-positive classification of speed score in the simulations and reiterate the prevalence of speed correlations in inhibitory neurons in the dorsal CA1 area of hippocampus in rats.

## 2 METHODS

### 2.1. METHOD DETAILS

We analyzed recordings of hippocampal neuronal activity made available by the Buzsaki Laboratory through the Collaborative Research in Computational Neuroscience data sharing website (http://crcns.or, hc-3 dataset). Detailed descriptions of the experimental procedures can be found in previous publications (DIBA; BUZSÁKI, 2008; MIZUSEKI et al., 2009, 2013, 2014). All protocols were aproved by the Intistutional Animal Care and Use Committee of Rutgers University. Below, we describe the analytical methods employed and, for convenience, also the relevant experimental procedures from the original publications (microdrive implantation, spatial arenas, data acquisition, spike detection and sorting and neuron type classification).

### 2.2. DATASET DESCRIPTION AND INCLUSION CRITEREA

There is a difference between dataset website description and provided data. We summarize relevant aspects to keep track of numerical differences that can be found between dataset description and the present analysis. The hc-3 dataset contains data from 11 male Long—Evans rats (250-400 g) of brain electrophysiology and animal movement along of 442 sessions in 14 different tasks. Animals were identified with tags, and database annotation asserts the position of each contact of implanted shanks. Description asserts 442 sessions, from which 297 sessions are provided with animal tracking files (.whl extension). As inclusion criteria we decided to utilize only the sessions that had at least one electrode contact in CA1 region, and that was recorded either in the square arena (46 sessions) or linear arena (80 sessions), 126 sessions in total. Only three animals remained after these filters, ‘ec013’ (38/75/113 sessions), ‘ec014’ (4/2/6 sessions), ‘ec016’ (4/3/7 sessions). Numbers in parenthesis depict the number sessions in square, linear and both arenas.

Data is “organized into top-level directories, each of which contains data for sessions recorded on the same day using the same animal and electrode placement combination.” - according to data-set description. Action potentials within the same top-level directory are stacked together in order to perform spike sorting for that particular animal/day. Cluster numbers were assigned to action potential waveform. Neuronal clusters were analyzed by Buzsáki laboratory and properties of these neurons have been reported in metadata ‘hc3-cell.csv’ file. However, not all data available with data-set were annotated nor vice-versa. Therefore, we adopted only neurons whose data was both provided and annotated.

Hippocampal sub-region on which shank was and the putative cell phenotype were the most relevant annotations that were applied into analysis. Phenotype was one of three that follows, pyramidal neuron, inhibitory neuron, non-class neuron; these were assessed according to waveform and rate of action potential emission. Another two phenotype were derived from first two, cross-correlation analysis (FUJISAWA et al., 2008) revealed the probable excitation or inhibition to a second recorded neuron indicating connectivity. These annotations will be briefly described in another section.

There were 1770 recorded neurons in dorsal hippocampus CA1 sub-region on either square or linear arenas. According to annotation, there were 1433 pyramidal neurons (842 | 591)[1], 221 inter-neurons (102 | 119)[1], and 116 non-class neurons. Besides region and task criteria, neuron were included only if their rate of action potential emission was higher than 0.3 Hz. This leaded to 1017 recorded neurons, 770 pyramidal (348 | 422)[1], 199 interneurons (84 | 115)[1] and 48 non-class neurons. In the linear arena, 705 recorded neurons, 519 pyramidal (196 | 323)[1], 151 interneurons (65 | 86)[1] and 35 non-class neurons. In the square arena 644 recorded neurons, 495 pyramidal (216 | 279)[1], 126 interneurons (49 | 77)[1] and 23 non-class neurons. Only 332 neurons were recorded on both arenas, which 219 of them were pyramidal (70 | 149)[1], 91 interneurons (42 | 49)[1] and 22 non-class neurons.

In animal ec013, there were 946 recorded neurons in dorsal hippocampus CA1 sub-region on either square or linear arenas. According to annotation, there were 702 pyramidal neurons (342 | 360)[1], 163 inter-neurons (84 | 79)[1],and 81 non-class neurons. Besides region and task criteria, neuron were included only if their rate of action potential emission was higher than 0.3 Hz. This leaded to 665 recorded neurons, 486 pyramidal (187 | 299)[1], 144 interneurons (69 | 75)[1] and 35 non-class neurons. In the linear arena, 567 recorded neurons, 414 pyramidal (150 | 264)[1], 125 interneurons (60 | 65)[1] and 28 non-class neurons. In the square arena 430 recorded neurons, 316 pyramidal (101 | 215)[1], 97 interneurons (39 | 58)[1] and 17 non-class neurons. Only 518 neurons were recorded on both arenas, which 388 of them were pyramidal (137 | 251)[1], 106 interneurons (48 | 58)[1] and 24 non-class neurons. Note that this animal is the one that have neuron record in both arenas.

In animal ec014, there were 429 recorded neurons in dorsal hippocampus CA1 sub-region on either square or linear arenas. According to annotation, there were 388 pyramidal neurons (277 | 111)[1], 29 inter-neurons (12 | 17)[1],and 12 non-class neurons. Besides region and task criteria, neuron were included only if their rate of action potential emission was higher than 0.3 Hz. This leaded to 209 recorded neurons, 177 pyramidal (113 | 64)[1], 26 interneurons (9 | 17)[1] and 6 non-class neurons. In the linear arena, 78 recorded neurons, 60 pyramidal (24 | 36)[1], 14 interneurons (3 | 11)[1] and 4 non-class neurons. In the square arena 131 recorded

neurons, 117 pyramidal (89 | 28)[1], 12 interneurons (6 | 6)[1] and 2 non-class neurons. None neurons were recorded in both arenas.

In animal ec016, there were 395 recorded neurons in dorsal hippocampus CA1 sub-region on either square or linear arenas. According to annotation, there were 343 pyramidal neurons (223 | 120)[1], 29 inter-neurons (6 | 23)[1],and 23 non-class neurons. Besides region and task criteria, neuron were included only if their rate of action potential emission was higher than 0.3 Hz. This leaded to 143 recorded neurons, 107 pyramidal (48 | 59)[1], 29 interneurons (6 | 23)[1] and 7 non-class neurons. In the linear arena, 60 recorded neurons, 45 pyramidal (22 | 23)[1], 12 interneurons (2 | 10)[1] and 3 non-class neurons. In the square arena 83 recorded neurons, 62 pyramidal (26 | 36)[1], 17 interneurons (4 | 13)[1] and 4 non-class neurons. None neurons were recorded in both arenas.

## 2.3. MICRODRIVE IMPLANTATION

Three male Long-Evans rats (250-400 g) were implanted with two silicon probes (200 um inter-shank distance) attached to individual microdrives; the first is a 4-shank probe in the entorhinal cortex and the second is either a 4 or 8-shank probe in the right dorsal hippocampus. Each shank had 8 recording sites (160 $\mu m^2$ each site; 1-3 MΩ impedance); in total with 64 recording sites on each implant. Shanks were aligned parallel to the septotemporal axis (angled at 45º parasagittal), and centrally positioned at -3.5 mm AP and 2.5 mm ML. Two stainless steel screws implanted above the cerebellum served as indifferent and ground electrodes. Shank positioning was verified histologically. After recovery from surgery (~1 week), physiological signals were recorded during different types of active waking behaviors.

## 2.4. SPATIAL ARENAS

From the hc-3 dataset we selected only those with task labeled as “bigSquare” or “linear”, here we re-label them as square and linear arenas. Accordingly, we analyzed CA1 activity from three rats recorded over 46 sessions in a 180-cm sided square arena, and 80 sessions in an elevated 7 cm wide and 250 cm long linear arena. In the square open-field arena, animals chased for randomly dispersed drops of water or pieces of froot loops (food); in the elevated linear arena, animals ran back and forth chasing for 30 μL water reward on both ends; animals were water-deprived for 24 hours prior to the experiment. Recordings were obtained after the animal was exposed ten or more training sessions to both arenas.

## 2.5. DATA ACQUISITON

Neuroelectrophysiological recordings were performed using a 128-channel DataMax system (16-bit resolution; RC Electronics). Signals were amplified (1,000 X), filtered between 1 and 5,000 Hz, and acquired continuously at 20,000 Hz. Local field potentials (LFPs) were obtained by decimating original signal to 1,250 Hz. Animal behavior was video-recorded through a camera mounted on the top of the arena (30 frames per second). The animal position was tracked from the XY coordinates of two light-emitting diodes of the headstage and was interpolated to match 1250 LFP samples in 32 frames (39.0625 Hz). Sessions were trimmed if the begining and end of tracking was missing data. Missing data within session was estimated as the linear interpolation of data at the edges of missing blocks of data.

## 2.6. SPIKE DETECTION AND SORTING

The original signals 20,000 Hz signal were filtered between 800 and 5,000 Hz and their root mean square (RMS) were computed. Spike detection threshold was defined as five times the stand deviation from the mean RMS over sliding windows of 0.2 ms. Waveforms of 32 or 48 samples around the peak were acquired and interpoolated to 40,000 Hz. Waveforms of same shank were stacked into a putative action potential signature with eight times samples of the original waveform. Signature of putative action potentials of the same day of experiment across multiple tasks were semi-automatically sorted by first using KlustaKwik software (http://klustakwik.sourceforge.net, (HARRIS et al., 2000), followed by manual adjustment of neuron clusters using Klusters software (http://klusters.sourceforge.net, (HAZAN; ZUGARO; BUZSÁKI, 2006). Only clusters with clear boundaries and refractory periods were considered as single units. Neuronal waveforms recorded on different days were clustered separately.

## 2.7. SPEED SCORE

The instantaneous animal speed was computed as the displacement of the animal tracking between two consecutive frames divided by the inter-frame interval (25.6 ms). The speed time-series was obtained by smoothing the instantaneous animal speed with a 1D-Gaussian with 250-ms standard deviation. The firing rate time series was obtained by smoothing spike counts over inter-frame intervals with the same Gaussian. The speed score of a neuron was defined as the Pearson's product-moment correlation coefficient (Pearson's r) between the time series of its firing rate and animal speed. In Figure 3, surrogate speed scores

were obtained by computing the Pearson's r between animal speed and the firing rate time series randomly circularly shifted between ± 90 seconds. Speed cells were operationally defined as neurons whose absolute speed score for the square arena was greater than 0.3. We opted to use this operational definition, which is more conservative than a surrogate-based threshold, because (1) the bimodality in the distribution of observed speed scores can be separated at 0.3 (see Figure 3A), and (2) a surrogate-based threshold (e.g., 4 SD from the surrogate mean) would give rise to speed cells with very low speed scores, which likely correspond to a by-product of place-field firing.

## 2.8. SCATTER PLOTS OF LOCOMOTION SPEED VERSUS FIRING RATE

For sake of visibility, the gray dots in the scatter plots of speed versus firing rate shown in figures 1D, 2C, 4B, 8A, 10A, 12A, and 13vi depicted only 10% of the data, selected at random. The black circles and lines display quantiles 25, 50 and 75 computed using all data within overlapping speed bins (width = 6 cm/s, step = 2 cm/s).

## 2.9. SPATIAL HEATMAPS

We applied heatmaps to visualize spatial dispersion of variables, matrices were result of the summation of 2D-Gaussians with 5-cm standard deviation centered at each XY tracking location with area under de curve equals to the variable value at each point. Variables analyzed were (1) occupancy, (2) animal speed, (3) rate of action potential emission. Heatmaps graphs were ploted using 100 x 100 bins. These heatmaps are shown in Figures

## 2.10. ANALYSIS OF SPEED SCORE STABILITY ACROSS SPACE AND TIME

To assess if speed score is stable across space and time in the square arena, we partitioned space in subregions and segmented time in blocks. Subregions were defined accoding two perspectives, (1) edge and center and (2) quadrants. Edge is defined as the 30-cm strip along the borders of the arena, center is a 120-cm sided central square; quadrants are 90-cm sided non-overlaping squares. Time segments were defined as 10-minute blocks non-overlaping time blocks for sessions with duration above 30 minutes, shorter sessions (10 min <= duration < 30 min) had three overlaping blocks with the centered at first five minutes, half of session, length of session minus five minutes.

## 2.11. SPEED-BINNED AUTOCORRELOGRAM

To compute the speed-binned autocorrelograms, first we linearly interpolated animal locomtion speed to match the LFP sampling rate (1,250 Hz), then we counted recorded action potentials at same rate. We binned speed into overlapping bins (width = 5 cm/s, step = 2 cm/s). For each speed bin, we only considered periods of at least 625-ms in which the animal's speed did not outmatch the corresponding speed rage for more than 125 ms. Next, for each selected period we computed the mean autocorrelograms of both LFP and spike count of periods within the same speed range. Finally, the speed-binned autocorrelograms were obtained by plotting the mean autocorelograms for each speed bin, normalized by it integral.

## 2.12. SPIKE COUNT PER THETA CYCLE

To compute the number of spikes per theta cycle, we bandpass filtered the LFP between 4 and 12 Hz. For each session, we selected the electrode with the highest theta power. The instantaneous theta phase was obtained from the analytical representation of the signal based on the Hilbert transform. Downward crossings defined boundaries between theta cycles. For each theta cycle, we computed the mean animal speed and the number of spike counts per neuron.

## 2.13. NEURON TYPE CLASSIFICATION

We inherited the neuronal type classification as provided along with the hc-3 data set, which was performed as described in (MIZUSEKI et al., 2009). In brief, hippocampal neurons were classified as either pyramidal neurons or interneurons based on waveform width, mean firing rates (CSICSVARI et al., 1999), and auto-correlograms (SIROTA et al., 2008) . Moreover, monosynaptic interactions between pairs of neurons were inferred by the analysis of cross-correlograms as described in detail in (FUJISAWA et al., 2008). In Figures 5, 6, 7, 9 and 14, we only considered neurons that were confirmed to be excitatory or inhibitory by the latter cross-correlogram analysis.

## 2.14. LINEAR DECODERS

In Figures 7 and 8, we built linear models using animal speed and firing rates as response and predictor variables (KROPFF et al., 2015). For these analyses, animal speed and

firing rates were averaged over 1-second non-overlapping bins. For each session, the first 350 samples were used for training the model and the following 150 samples for testing. In Figure 7D, the number of neurons employed varied from one to four in a given session. The number of models for each session was determined by all possible combinations of cells. For each model, the "decoding accuracy" was defined as the Person's r squared ($r^2$) computed between observed and predicted speeds. In Figure 8, training and testing samples were derived from either the same or different sessions, as labeled; the mean decoding error was defined as the average difference between predicted and observed speeds. In Figure 7E, before computing single cell decoding accuracy and speed scores as above, we randomly down-sampled spikes in order to make the two cell types have the same average firing rate, as indicated in the X axis. This procedure was performed 100 times for each cell and fixed firing rate value. For the statistical analysis (mean, SEM and t-test), we used the average value of a cell as a sample.

## 2.15. COMPUTATIONAL MODELS OF PLACE AND SPEED CELLS

We used original behavioral data (position and speed) to simulate the instantaneous firing rate of model place and speed cells, derived from a Poisson process of mean $\lambda$. For each recorded session, the animal position was binned into 10-cm wide bins and the instantaneous speed into 8 quantiles. For model place cells, the mean firing rate ($\bar{\lambda}_{place}$) was solely a function of space, determined by a "spatial tuning curve". For model speed cells, the mean firing rate ($\bar{\lambda}_{speed}$) was a function of speed, determined by a "speed tuning curve". Different model cells were simulated using different tuning parameters. In the square arena, the spatial tunings were 2D-Gaussians with center coordinates $(x,y)\in\{(90,90),(126,54),(18,90),(18,18)\}$ (cm,cm) and standard deviation $(\sigma_x,\sigma_y)\in$¿ ¿ $\{(45,45),(27,27),(9,9)\}$ (cm,cm); in the linear arena, we used 1D-Gaussians with $x\in$¿ ¿ $\{70,125,236\}$ cm and $\sigma_x\in\{45,27,9\}$ cm. The speed tuning curves were sigmoid functions with rising constant of 20 cm/s and half constant $speed_{50}\in\{20,35,50\}$ cm/s in the square arena and ϵ {20, 45, 70} cm/s in the linear arena. Finally, for both $\lambda_{speed}$ and $\lambda_{place}$, the tuning curves were normalized such that the maximal and minimal values $(fr_{min},fr_{max})\in\{(0,1),(0,10),(0,40),(40,80)\}$ (Hz,Hz). In Figures 11 to 13, we also investigated mixed neuron types, in which the mean firing rate was first set to $\lambda_{s:p}=s*\lambda_{speed}+p*\lambda_{place}$ ,with $(s,p)\in\{(4,0),(3,1),(2,2),(1,3),(0,4)\}$ and then normalized to achieve the desired

$(\lambda_{min}, \lambda_{max})$ values. Simulated firing rates were analyzed in the same way as the actual firing rates.

## 2.16. LINEAR-NONLINEAR ALGORITHM

As a control to the ethological interdependece of spatial position and locomotion speed (e.g., speed is lowest on the edges of the linear arena), in Figures 13 and 14 we used the linear-nonlinear (LN) statistical model described in (HARDCASTLE et al., 2017). LN models can be used to quantify the dependence of the firing rate on position and speed isolatedly or in combination (HARDCASTLE et al., 2017). Briefnly, LN models estimate the mean firing rate of a neuron as function of the exponential of the weighted sum of the partitions of the analyzed variables. For models that take into account both position and speed, mean neuronal activity is estimated as:

$$\bar{R} = \exp\left(w_{place} * P + w_{speed} * S\right)$$

while $R_{place} = \exp\left(w_{place} * P\right)$ or $R_{speed} = \exp\left(w_{speed} * P\right)$ for single variable models. **R** is a $R \in \mathbb{R}^{Tx1}$ of mean firing rate values, T is the number of 25.6-ms time bins, $P \in 1^{TxN_{place}}$, where $N_{place}$ is the number of spatial partitions ( $N_{place}$ = 36 and 50 on square and linear arenas, respectively), and 1 is the indicator function that assumes value of one at the time bin if the variable value is within partition interval, zero otherwise; and $S \in 1^{TxN_{speed}}$, where $N_{speed}$ is the number of speed intervals. The weight vectors $w_{place} \in \mathbb{R}^{N_{place} x1}$ and $w_{speed} \in \mathbb{R}^{N_{speed} x1}$ are the weight column vectors with the same number of partitions. These weights are learned through an optmization algorithm that maximizes the Poisson log-likelihood (HARDCASTLE et al., 2017). Predicting firing rate series are generated through Poisson process with mean firing rate parameter at each time bin determined by $R$. Model performance is characterized by the log-likelihood increase (LLHi) of the data under the model in relation to a Poisson model of fixed firing rate, and by the accuracy ($r^2$) of the model in predicting the real spiking activity of the neuron. To compute the latter, the spike counts generated by the model were smoothed as the actual data. Implementation was done by adapting codes available at https://github.com/GiocomoLab/ln-model-of-mec-neurons/ (last commit on 29 October 2017).

## 2.17. QUANTIFICATION AND STATISTICAL ANALYSIS

Speed scores were defined as the Pearson product-moment correlation coefficient between the time series of locomotion speed and firing rate. The surrogate distributions of speed scores shown in Figure 3 were obtained by computing the Pearson correlation coefficient between animal speed and the firing rate time series randomly circularly shifted between ± 90 seconds. Speed cells were operationally defined as neurons whose absolute speed score was higher than 0.3. The p-values associated with the Pearson's correlation coefficients shown in Figures 1D, 2C,D and 4C were obtained using Student's t distributions (function corr.m in MATLAB). The cross-correlation lags in Figure 6 were compared against zero using one-sample t-tests. Mean decoding accuracy obtained for pyramidal cells and interneurons (Figure 7D,E) was compared with two-sample t-tests. In Figure 9C, the speed scores for the preferred and non-preferred directions were compared with paired t-tests; the proportion of bidirectional speed cells among interneurons and pyramidal cells were compared using a chi-square test. In all statistical analyses, $p<0.05$ was considered to be statistically significant. Unless noted otherwise, data from individual neurons were considered as samples.

# 3 RESULTS

## 3.1. NEURONAL CORRELATES OF LOCOMOTION SPEED

To investigate neuronal correlates of locomotion speed in the hippocampus, we analyzed the neuroelectrophysiological activity of CA1 neurons of hippocampus in freely moving rats (n=3 rats). Rats were recorded in a square arena (n=46 sessions) searching for randomly-dispersed froot loops; and in the linear arena (n=80 sessions) chasing water at both ends. Figure 1 demonstrate a representative example a neuronal correlate of speed in the square arena. Figure 1A shows an animal trajectory plotted along with 10% of the action potentials of a CA1 neuron; note that this neuron was activated all over the arena. Figure 1B depicts heat-maps of spatial distribution of (1) animal occupancy time, (2) animal speed, and (3) neuron firing rate. It is noticeable that the animal occupied most of the time two different spots indicated by either the warm colors in elapsed time heatmap – high occupancy time – or the cold colors in the speed – low speed. A first clue of speed correlation was hinted as the firing rate heatmap is slowest in these same locations. Inspection of time dynamics of speed and firing rate is displayed in Figure 1C, time series of speed (top) and a neuron firing rate (mid) and z-score of both (bottom) are shown; suggesting that these two variables are correlated in a sub-second timescale. Scatter plot in Figure 1D shows the collapsed time of both variables, speed bin-averaged firing rate are shown with lines ($1^{st}$, $2^{nd}$ and $3^{rd}$ quartiles); inset text depicts the value of speed score ($r=0.62$, $p<10^{-20}$) (KROPFF et al., 2015), defined as the Pearson's r coefficient (r) between speed and firing rate (see Material and Methods).

To evaluate the consistence of speed correlates of CA1 neurons across space and time, we segmented data in interval partitions. In Figure 2, we present a second example of CA1 neuron correlated with speed during a 90-minute long session in the square arena. Figure 2A displays heat-maps of speed and firing rate, visual inspection corroborates the correlation as in Figure 1B. Spatial partitions are defined in Figure 2B: whole arena (W), four quadrands (Q1, Q2, Q3, Q4), edge (E), and center (C). Scatter plots of whole arena and data restrained within each spatial partition are present in Figure 2C, speed score metric indicate a stable ($r=0.60\pm0.04$) across space. Thereafter, to investigate the stability of speed score across time we partitioned time in 10-minute non-overlapping intervals (Figure 2D). The leftmost plot in Figure 2D displays the variation of speed score across time ($r=0.68\pm0.04$) utilizing the whole session data, this demonstrated the stability of time. The remain plots of Figure 2D utilizes data in the intersection of space and time partitions intervals to demonstrate that speed score ($r=0.58\pm0.11$, across space and time intervals) is stable across space and time.

Figure 1 – Locomotion speed neuronal correlate in CA1 area of dorsal hippocampus

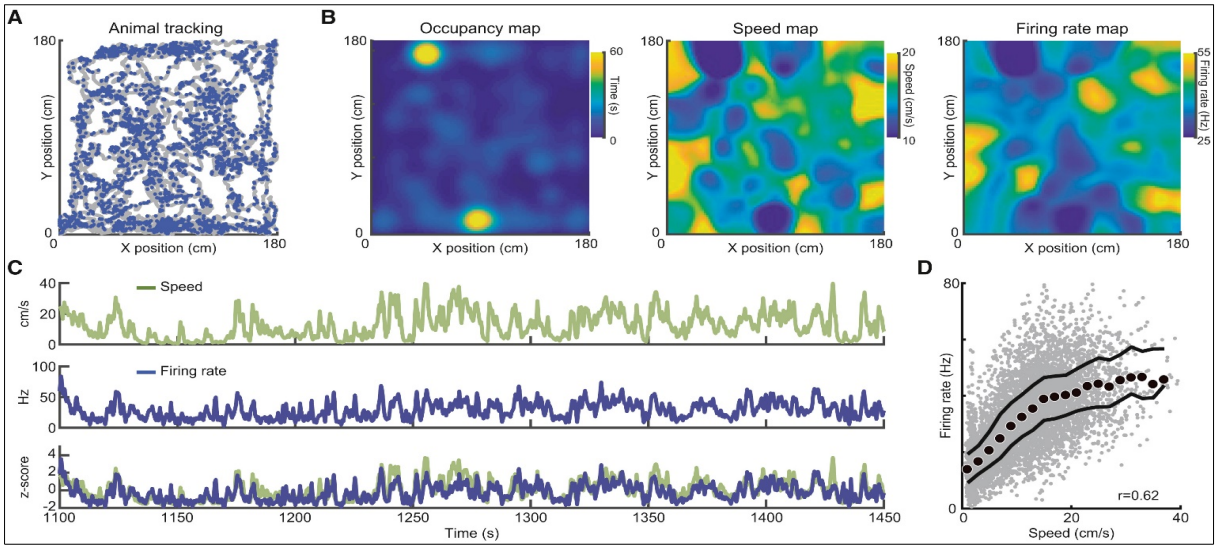


**Figure 1:** ***(A)*** Gray line depicts animal trajectory in a square open-field arena and blue dots action potentials of a CA1 neuron; ***(B)*** Heat-maps of spatial distribution of (left) elapsed time, (middle) speed, and (right) firing rate of the same session and neuron; ***(C)*** Time series of speed (top) and neuron firing rate (middle), and z-scored transformation of both (bottom); ***(D)*** Scatter plot of speed and firing rate in gray, speed-binned in black are median circles and 25% and 75% quartiles lines. Inset text is this neuron speed score. **P.S.:** Only random-selected 10% of data is shown in A and D for better visualization.

The example neurons in Figures 1 and 2 are representative of a subpopulation of CA1 neurons, hereafter referred to as "speed cells" - a brief though on this jargon usage is in the discussion section. This subpopulation was described from the 644 CA1 neurons whose average rate of action potential emission was higher than 0.3 Hz while the animal was foraging the square arena. Speed score distribution of CA1 neurons is bimodal, with a prominent peak near 0 and a smaller bump centered around 0.45 (Figure 3A). In this work, we operationally defined "speed cells" as neurons having absolute speed score greater than 0.3. Figure 3B sows three examples of surrogate distributions of speed scores (see Method Details) along with the actual speed score for cells whose firing rate had non-significant (top), negative (middle) and positive (bottom) correlations with speed. At the group level, the observed distribution of speed scores was skewed to the right compared to the pooled distribution of surrogate speed scores (Figure 3A). In our perspective, the operational definition with the chosen threshold is more conservative than a definition solely based on surrogate distributions (Figure 3A,B). The base of this perspective are: (1) the threshold separated the bimodal distribution of speed scores (Figure 3A); (2) all absolute speed scores above this threshold were highly significant when compared to surrogate distributions; and (3) we wanted to avoid spurius correlations due to spatial influences such as place field traversals. Clearly, place cells spike at higher rates when the animal runs across the place field than during immobility; in turn, this leads to weak correlations between firing rate and speed that are deemed significant by surrogate-based statistics. Under this more stringent definition, we found that 93/644 (14%) of CA1 neurons were speed cells. As the example cell in Figure 2,

the vast majority of defined speed cells were stable across time (Figure 3C) and space (Figure 3D).

Figure 2 – Locomotion speed correlate in CA1 is stable across space and time

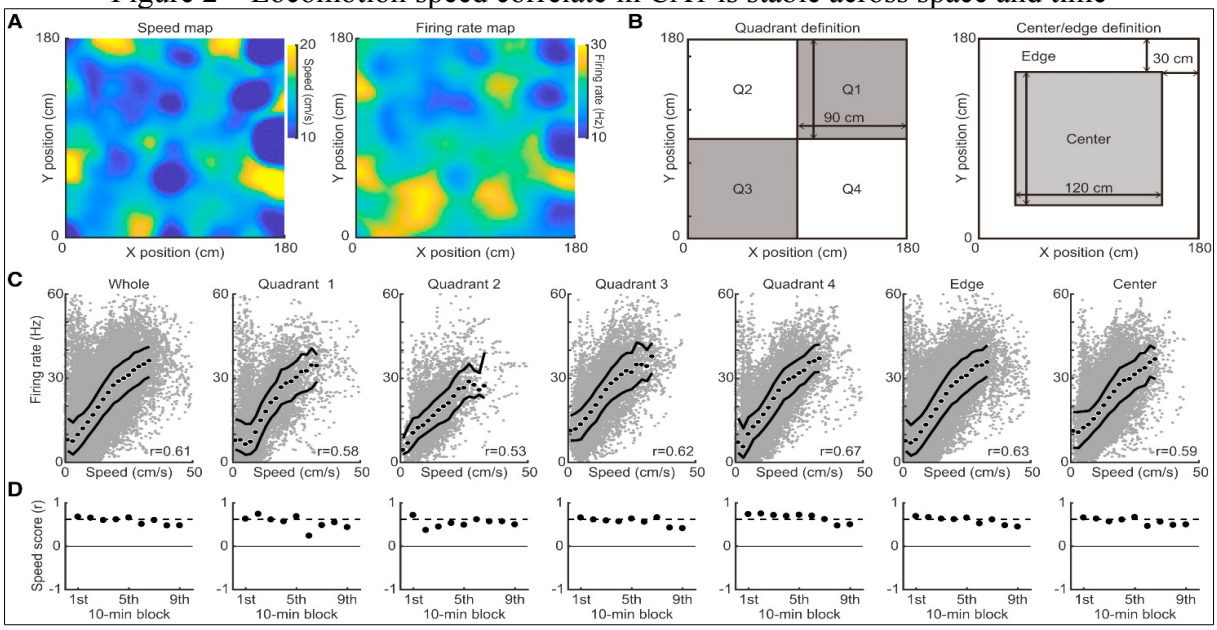


**Figure 2:** ***(A)*** Heatmaps of spatial distribution of speed and firing rate of a CA1 neuron. ***(B)*** Diagram of spatial partitions in the square arena: whole arena (W), quadrants (Q1,Q2,Q3,and Q4), edge (E), center (C). ***(C)*** Scatter plot of speed and of firing rate as in Figure 1D; ***(D)*** Time binned speed score over 10-minute-block time segments for each spatial partition defined in Figure 2B, dashed line is the whole session speed score. **Note:** Only random-selected 10% of data is shown in A and D for better visualization.

## 3.2. SPEED CORRELATION WITHIN THETA CYCLES

Theta oscillations (5-10 Hz) robustly appear in hippocampal local field potentials (LFPs) when rats perform voluntary movements (BUZSÁKI, 2005; BUZSÁKI; MOSER, 2013). Previous studies have shown that the frequency of the LFP theta rhythm increases with speed (SŁAWIŃSKA; KASICKI, 1998; HINMAN et al., 2011). Moreover, it has also been well documented that the spiking activity of hippocampal neurons may oscillate at theta frequency and that the LFP theta phase modulates spiking probability (FRANK; BROWN; WILSON, 2001; BUZSÁKI, 2002; KLAUSBERGER et al., 2003). Therefore, changes in rate of action potential emission of CA1 speed cells may be a consequence of changes in theta frequency with speed, in which a higher number of theta cycles per unit of time would lead to a higher number of action potential emission per unit of time, an effect reffered to as "oscillatory coding" (HINMAN et al., 2016). Alternatively, the increase of rate of action potential emission with speed can occur within theta cycles. In this cenario, CA1 speed cells would emit more action potentials per theta cycle as a funtion of speed despite of the instantaneous theta frequency, which defines the "rate coding" (HINMAN et al., 2016). We

next investigated whether rate coding would underlie the emission rate changes of CA1 speed cells.

Figure 3 – Speed score distribution over dorsal hippocampal in CA1 neurons

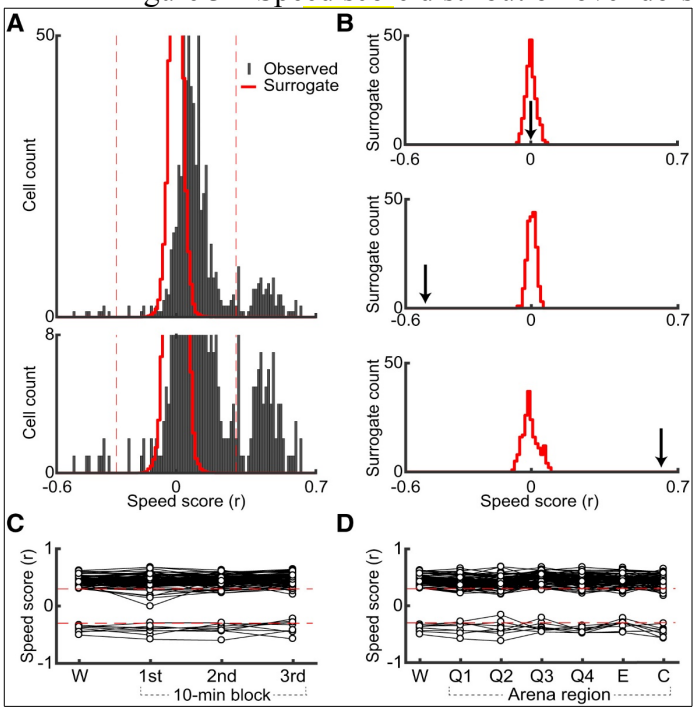


**Figure 3:** ***(A)*** Speed score histogram of CA1 neurons in square arena sessions. Red line is the speed score histogram of circular-shifted firing rate time series. Dashed lines indicate ±0.3 speed score threshold – cells whose speed score are above/bellow threshold are defined as speeed cells. Bottom graph is a y-axis zoom of top to highlight bimodal distribution. ***(B)*** Three cells examples whose speed scores (black arrows) are either in between, below, or above thresholds; along with with each 1000-surrogate curves. ***(C)*** Time stability of speed cells' speed score in square arena over 1st, middle and last 10-block time segments. ***(D)*** Same as in (C) for spatial segmentation of square arena partitions.

The top panel of Figure 4A shows the standard autocorrelogram of a CA1 speed cell exhibiting theta-rhythmic firing, and the middle panel shows the speed-binned auto-correlogram, which depicts normalized spiking probabilities for different speeds (see Method Details). Notice that theta-rhythmic firing by this neuron occurred at all speeds. Moreover, as with the LFP theta rhythm (Figure 4A bottom panel), theta-rhythmic firing increased in frequency with speed (as inferred from the shorter period between the probability peaks), suggestive of oscillatory coding (HINMAN et al., 2016). Nevertheless, to test for rate coding, we next counted the number spikes emitted per theta cycle when controlling for speed. As shown in Figure 4B, the spike count per theta cycle increased with animal speed; moreover, such increase was proportional to the increase in firing rate with speed. This example neuron is representative of the population of CA1 speed cells. Namely, at the group level, we found that the slope of spike counts per theta cycle vs. speed was positive and highly correlated with the slope of firing rate vs. speed ($r=0.98$, $p<10^{-40}$) (Figure 4C). Therefore, we conclude that CA1 speed cells display a genuine rate coding of speed: their firing rate increases proportional to speed irrespective of changes in LFP theta frequency.

Figure 4 – Speed cells increase spike emission per theta cycle with speed

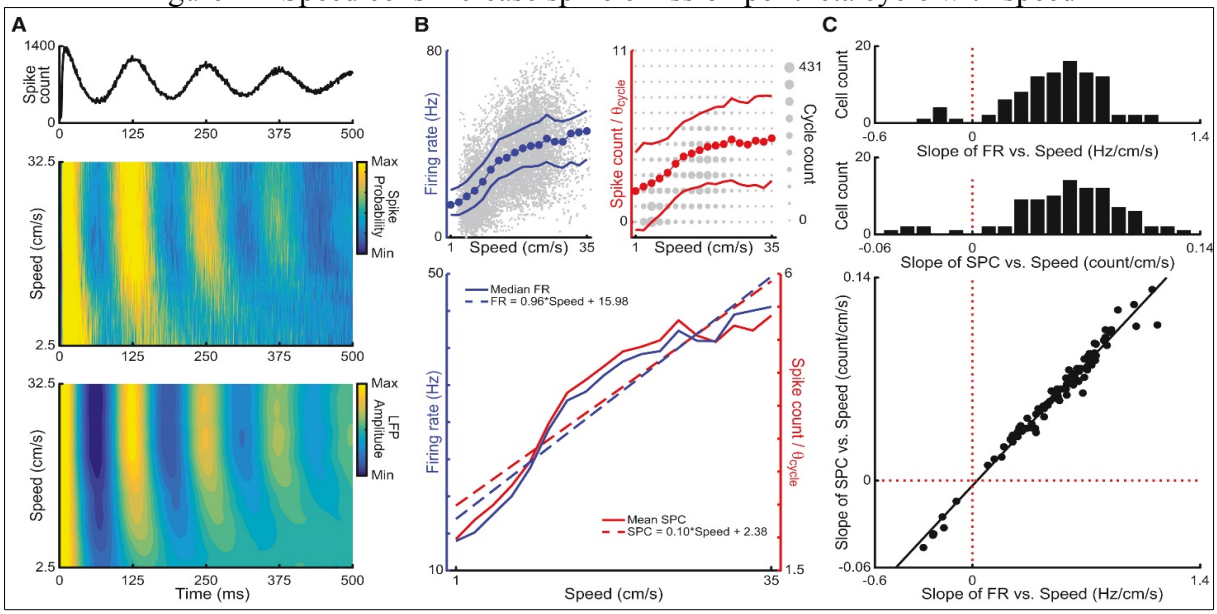


**Figure 4:** ***(A)*** Standard (top) and speed-binned (middle) autocorrelograms of a CA1 speed cells; the speed-binned LFP autocorrelogram is also shown (bottom). ***(B)*** The top panels show scatter plots of firing rate (FR, left) vs. speed and of spikes per theta cycle (SPC, right) vs. speed for a representative speed cell. In the right plot, circle size represents the number of theta cycles. The bottom panel shows median FR (blue) and mean SPC (red) as functions of speed; dashed lines show the linear fit. ***(C)*** Distributions of the slopes of the linear fit between speed and median FR (top) and between speed and mean SPC (middle) for all CA1 speed cells, and their scatter plot (bottom).

## 3.3. CA1 LOCOMOTION SPEED CORRELATED CELLS ARE INTERNEURONS

The firing rate maps of the representative CA1 speed cells in Figures 1 and 2 show that spikes occurred all over the square open-field arena. Moreover, notice in the scatter plots of Figures 1, 2 and 4 that all example CA1 speed cells displayed high firing rate. Low spatial selectively and high firing rate characterize the spiking activity of inhibitory interneurons in CA1 (FRANK; BROWN; WILSON, 2001). In contrast, CA1 pyramidal cells tend to emit low-frequency spikes with higher spatial information (MCNAUGHTON; BARNES; O'KEEFE, 1983; FRANK; BROWN; WILSON, 2001). These observations strongly suggest that CA1 speed cells are interneurons. To investigate this possibility, we used an identification of pyramidal cells and interneurons based on spike cross-correlograms (CCG, Figure 5A; (FUJISAWA et al., 2008; MIZUSEKI et al., 2009). Figure 5B-F shows results obtained for all pyramidal neurons and interneurons recorded in the square open-field arena that could be identified under the CCG analysis. As expected, neurons physiologically identified as interneurons had higher firing rate and narrower spike width than neurons identified as pyramidal cells (Figure 5B). Interestingly, we found that virtually all CA1 units classified as speed cells in the square arena were interneurons (Figure 5C-F). Accordingly, from a total of 77 cells physiologically identified as CA1 interneurons, 61 (79%) were considered speed

cells. In contrast, only one of the 279 (0.36%) physiologically identified pyramidal cells was classified as speed cell in the square arena (Figure 5F).

Figure 5 – Speed cells are interneurons

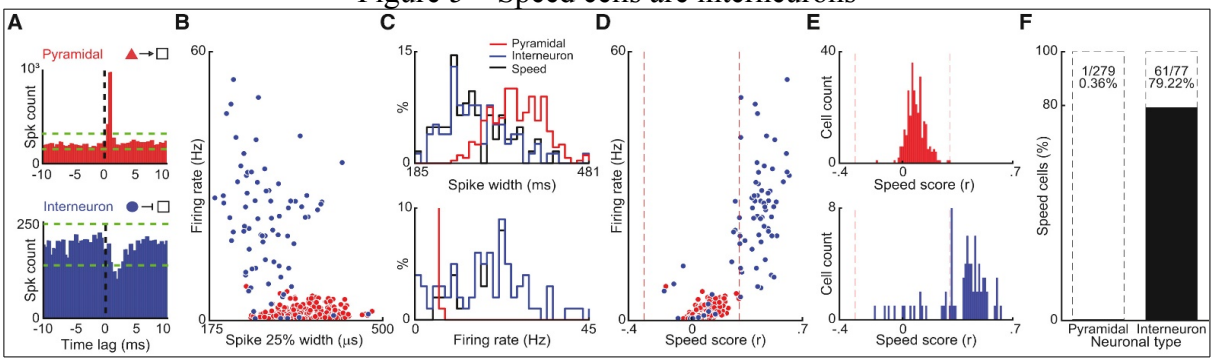


**Figure 5:** ***(A)*** Spike cross-correlograms for reference units (spike at 0) identified as pyramidal cell (top) and interneuron (bottom). Adapted from Mizuseki et al. (2009). ***(B)*** Scatter plot of spike width vs. firing rate for pyramidal cells (red) and interneurons (blue). ***(C)*** Distributions of spike width (top) **and** firing rate (bottom) for pyramidal cells (red), interneurons (blue), and speed cells (black). ***(D*** and ***E)*** Scatter plot of speed score vs. firing rate *(D)* and speed score distributions *(E)* for pyramidal cells (red) and interneurons (blue) recorded in the square open-field arena. ***(F)*** Proportion of speed cells in the square arena among physiologically identified neurons.

Cross-correlations between the time series of firing rate and speed further revealed that the firing rate changes of CA1 speed cells lagged changes in speed by 64.8±22.9 ms, which was significantly different from zero ($t(61)=-2.826$, $p=0.0064$; Figure 6). On the other hand, neurons not classified as speed cells had a mean lag between firing rate and speed not statistically different from 0 (pyramidal cells: $t(277)=0.768$, $p=0.44$; other interneurons: $t(15)=-2.105$, $p=0.053$), though these cells exhibited a much wider distribution of cross-correlation lag values than the speed cells (Figure 6). In all, we conclude that CA1 speed cells are interneurons, and that their firing rate tends to follow – more than lead – changes in speed.

## 3.4. PYRAMIDAL CELLS DO NOT ENCODE BUT ARE MODULATED BY SPEED.

Earlier studies have consistently shown that the firing rate of pyramidal cells increases with speed (MCNAUGHTON; BARNES; O'KEEFE, 1983; WIENER; PAUL; EICHENBAUM, 1989; CSICSVARI et al., 1999; HIRASE et al., 1999; EKSTROM et al., 2001; MAURER et al., 2005). Therefore, at first glance the results above – which indicate that pyramidal cells are not speed cells – seem to be at odds with previous literature. However, it should be noted that here we have measured the correlation between the time series of instantaneous firing rate and speed, which has recently been used to define speed cells in the medial entorhinal cortex (KROPFF et al., 2015). This contrasts with the cited studies which have measured the *average* firing rate of pyramidal cells as a function of speed, but have not assessed for firing rate correlations with speed at the timescale of animal behavior.

Figure 6 – Speed cells repeat speed after a delay

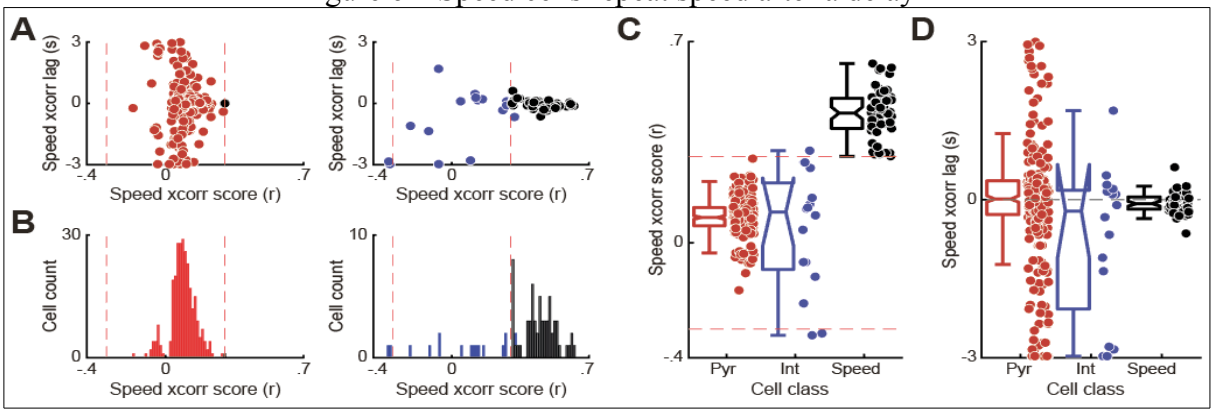


**Figure 6:** ***(A)*** Scatter plots of the time lag ("speed xcorr lag") vs. the peak ("speed xcorr score") of the cross-correlation between firing rate and locomotion speed, shown separately for physiologically identified pyramidal cells (left) and interneurons (right). Units classified as speed cells in the square open-field arena by the standard speed score (xcorr at 0 lag) are shown in black, whereas other interneurons and pyramidal cells (i.e., non-speed cells) are shown in red and blue, respectively. ***(B)*** Histogram counts of speed xcorr scores. ***(C*** and ***D)*** Boxplot distributions of speed xcorr score *(C)* and speed xcorr lag *(D)* for speed cells ("Speed") as well as for other interneurons ("Int") and pyramidal cells ("Pyr") that are not speed cells.

As shown in Figure 7A,B, we were able to reproduce the dependency of the average firing rate of CA1 pyramidal cells on speed when analyzing square arena sessions, thus consistent with previous studies (MCNAUGHTON; BARNES; O'KEEFE, 1983; WIENER; PAUL; EICHENBAUM, 1989; CSICSVARI et al., 1999; HIRASE et al., 1999; EKSTROM et al., 2001; MAURER et al., 2005). However, notice in Figure 7A that while the average firing rate is highly modulated by speed (red lines), no apparent correlation can be inferred from the scatter plots of instantaneous speed vs. firing rate (gray dots; compare with the scatter plots of speed cells in Figures 1, 2 and 4). Therefore, while we could confirm that the firing rate of pyramidal cells depends on speed, our results also show that pyramidal cell activity at best only weakly correlates with instantaneous changes in speed in the open field (Figures 5D,E and 7A).

To further elucidate this matter, we next investigated whether it was possible to decode the time series of animal speed from CA1 neuronal activity using linear decoders (see KROPFF et al., 2015 and Method Details). As expected, locomotion speed could be well decoded from the instantaneous firing rate of CA1 units defined as speed cells, and decoding accuracy tended to increase with the number of analyzed speed cells (Figure 8C,D; see also Figure 11). On the other hand, locomotion speed in the square open-field arena could not be properly decoded from the instantaneous firing rate of pyramidal cells (Figure 8C). Accordingly, decoding accuracy was much lower when using the firing rate of pyramidal cells compared to speed cells, irrespective of the number of analyzed cells (Figure 8D). Interestingly, speed cells exhibited higher speed scores and decoded speed better even after down-sampling spikes in such a way as to make them have the same low firing rates as

pyramidal cells (Figure 8E). Therefore, despite the increase in average firing rate with speed exhibited by both interneurons and pyramidal cells (Figure 8B; see also MAURER et al., 2005), we conclude that, in the open field, only interneurons that are speed cells, but not pyramidal cells, can accurately encode speed at the sub-second timescale.

Figure 7 – Pyramidal cells do not encode but are modulated by speed.

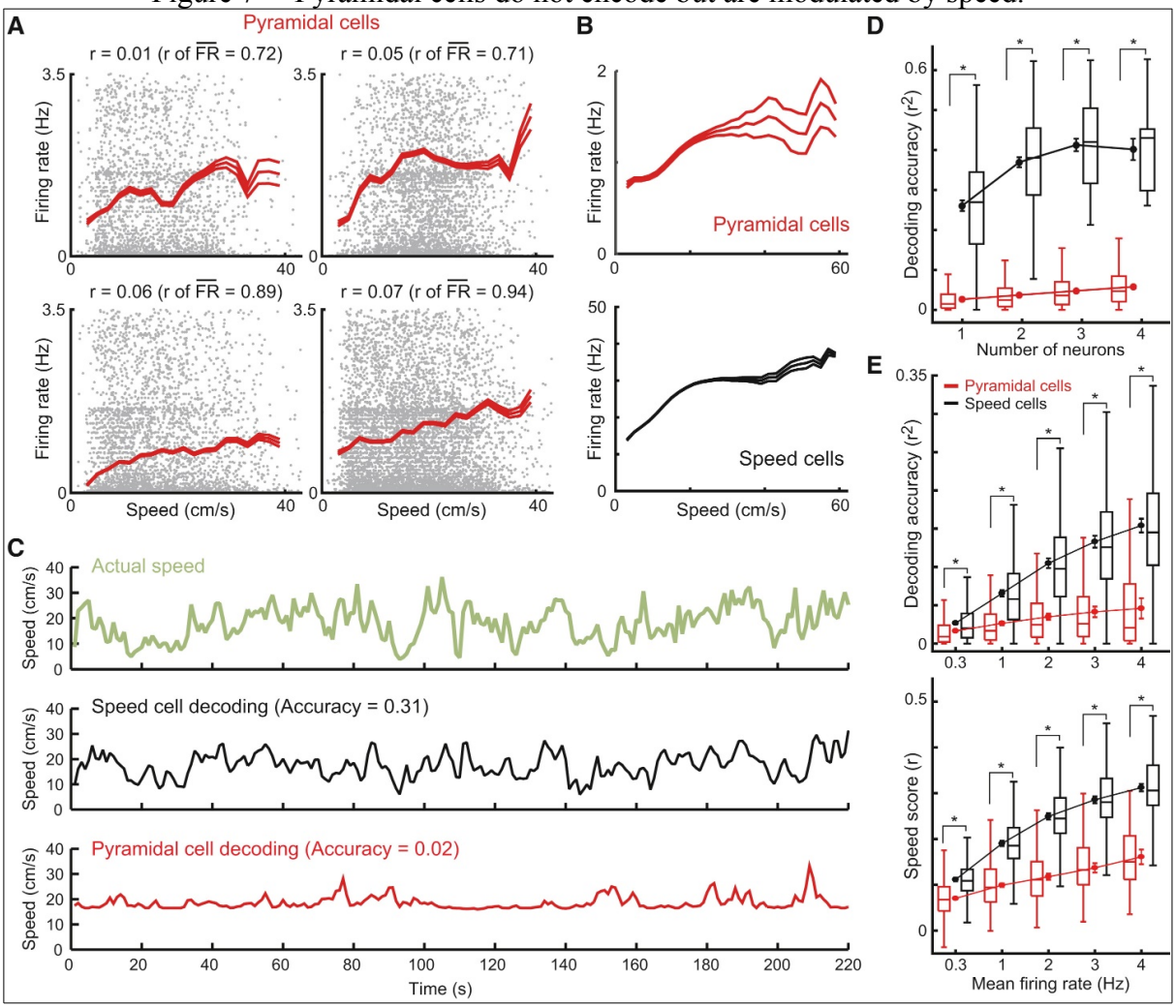


**Figure 7:** ***(A)*** Scatter plots of animal speed vs. firing rate (gray dots) for four example pyramidal cells recorded in the square open-field arena. The red lines show the mean firing rate (±SEM). For each panel, the title indicates the speed score (i.e., the correlation coefficient between the instantaneous firing rate and speed) and the correlation coefficient of the mean firing rate $\left(\overline{FR}\right)$ vs speed.***(B)*** Group data of mean firing rate (±SEM) as a function of locomotion speed in the open field. ***(C)*** Top panel shows the time series of locomotion speed in the open field. Bottom panels show examples of decoded speed from the firing rate of one speed cell (black) and one pyramidal cell (red). ***(D)*** Boxplot distributions of speed decoding accuracy for pyramidal (red) and speed cells (black) recorded in the square open-field arena. Connected circles show mean ± SEM. Decoding accuracy is defined as the square of the correlation between the decoded and the actual speed time series (i.e., the coefficient of determination). *p<0.00001. ***(E)*** Boxplot distributions of speed scores (bottom) and speed decoding accuracy (top) for individual pyramidal (red) and speed cells (black) after down-sampling spikes to make the two cell types have the same firing rate (see Method Details). Connected circles show mean ± SEM over cells. *p<0.00001.

## 3.5. PYRAMIDAL CELLS SPURIOUS CORRELATES SPEED IN LINEAR TRACK

Figures 1 to 7 showed results for CA1 neurons recorded from animals wandering in the square open-field arena. To evaluate consistence of neuronal correlates of speed in the hippocampus, we analyzed the persistence of it in different contexts. There are substantial differences in the ethological display among square and linear arenas. In the square arena, the animal have a broader area to forage, and the scattered froot loops task is an unpredictable task which objective is to be perceived around the environment. In the linear arena, the animal have a smaller area to forage, and the objective is well defined at both ends of arena; therefore, the animal doesn't exitate to run towards the reward region at both ends of the arena. In Figure 8, we demonstrate the speed profile of rats locomotion speed in the square and linear arenas. In bottom row of Figure 8 we can perceive that animals display lower speeds in the square arena than in the linear arena, while higher speeds are elicited in linear arena comparing to the square arena.

Figure 8 – Difference on locomotion speed profiles among square and linear arenas

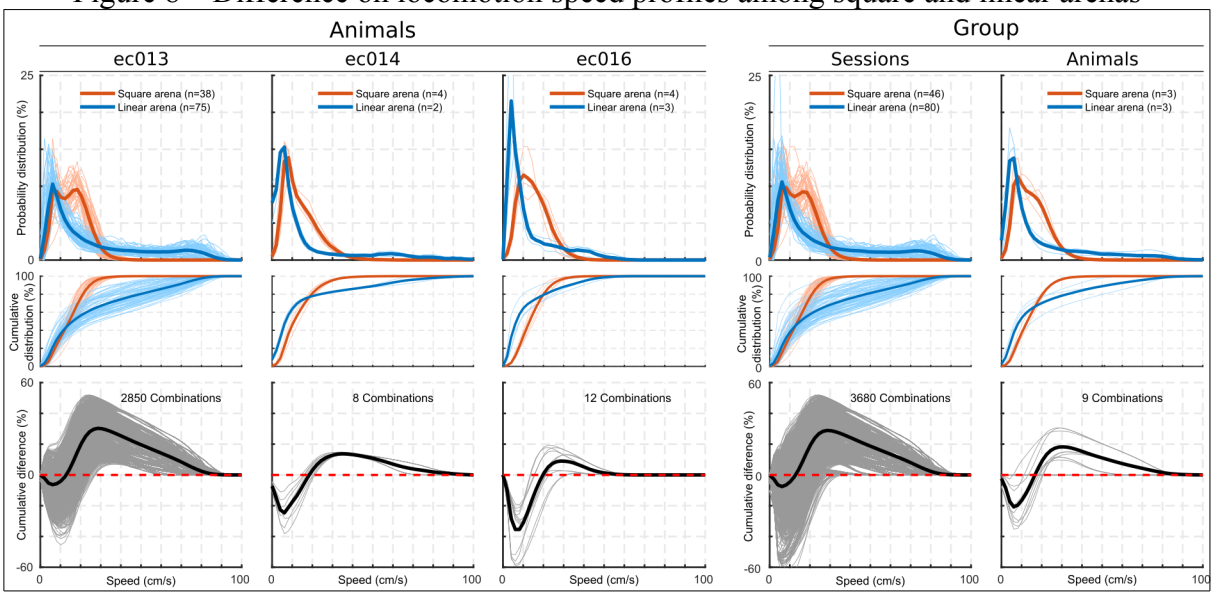


**Figure 8: (top)** Locomotion speed histograms for each animal, and group result of all sessions and mean of animals sessions. Thick lines display the mean for sessions of the same arena which are indicated with color, thin lines are individual sessions histograms. Thin lines in the animal group are the mean over sessions for each rat. **(middle)** Cumulative distribution of *(top)* distributions. **(bottom)** Difference of linear and square arenas cumulative speed distributions, thin lines are pair wise difference and thick lines are the mean difference, but in animal group on which thin lines are pair wise differences of the mean cumulative distributions of each animal and thick is the mean of these.

Moreover, by restricting the analysis to neurons that were recorded within the same day in both the square and linear arenas, we found that 82% of speed cells classified in the square arena were also considered speed cells in the linear track (Figure 9). Therefore, these results indicate that speed coding in the dorsal CA1 is stable across different contexts.

Figure 9 – CA1 speed cells defined in square arena persist correlates in linear arena.

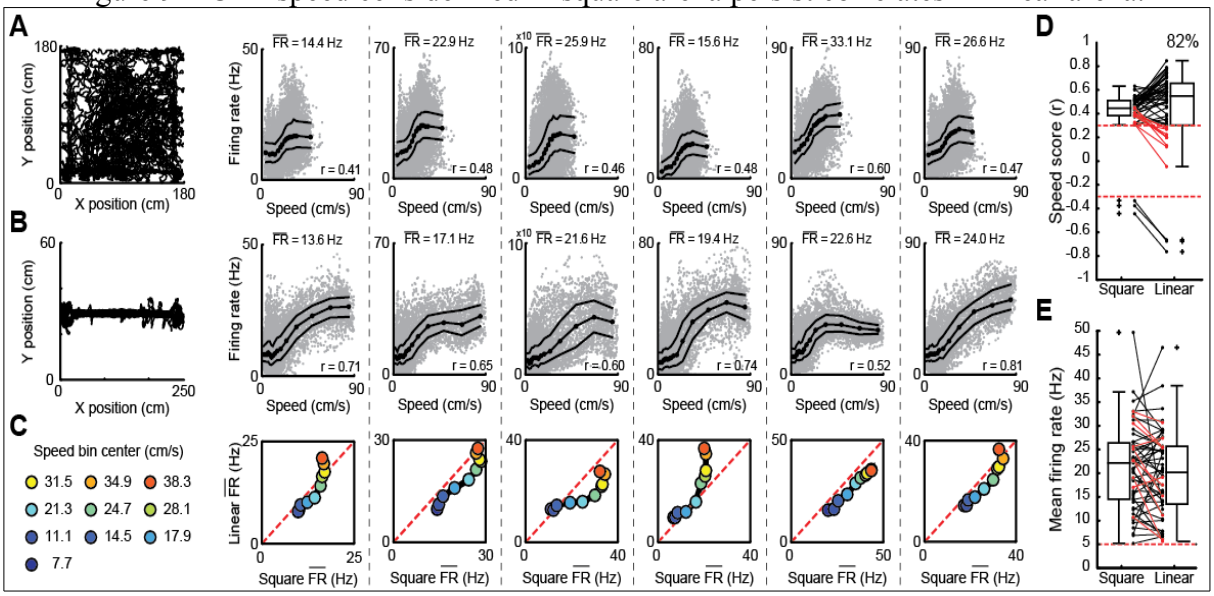


**Figure 9:** ***(A, B)*** Animal tracking and scatter plots of speed vs. firing rate of six CA1 speed cells recorded in the same day in the square (ec013.858) and linear (ec013.859) arenas. Black circles and lines show the median and 25-75% quartiles for each speed bin. Inset texts indicate speed scores (all p's<$10^{-20}$); the titles state the mean firing rate $(\overline{FR})$. ***(C)*** Scatter plots of speed binned $\overline{FR}$ in the square vs. linear arenas (same cells as in *A* and *B*). Colors indicate speed bin centers (bin width = 3.4 cm/s). ***(D)*** Boxplot of speed scores in the square and linear arenas for CA1 speed cells defined in the square arena; 82% of the cells were also considered speed cells in the linear track (red lines mark unstable cells). ***(E)*** Boxplot of $\overline{FR}$ for the same cells as in *D*. **Note:** Only cells with firing rate > 5 Hz in both arenas were taken into account.

In Figure 10, action potential time series of speed cells were utilized to evaluate the capacity to decode speed across tasks. We demonstrate that least squares applied can be applied to fit linear coefficients that can transform speed cells action potential activity to estimate locomotion. We applied this linear fitting with speed cell data from both square and linear arenas. Fitting were performed in three different configurations utilizing data of (1) a same trial; (2) different trial, same task; (3) different trial, different task. Figure 10A demonstrate that increasing number of neurons in the decoding may increase the decoding accuracy (see Material and Methods) up to a plateau. Moreover, the ethological differences (Figure 8) directly influence decoding across different tasks. In Figure 10A bottom two rows demonstrate that decoding accuracy across arenas is feasible; however, this metric is related to co-variance of both signals and the amplitude of predicted signal is discrepant as the range of speed is different in both tasks. It becomes clear in Figure 10B bottom two lines where the decoding error is negative in square-linear decoding, while positive in the linear-square decoding.

Figure 10 – CA1 speed cells firing rate decoding of speed

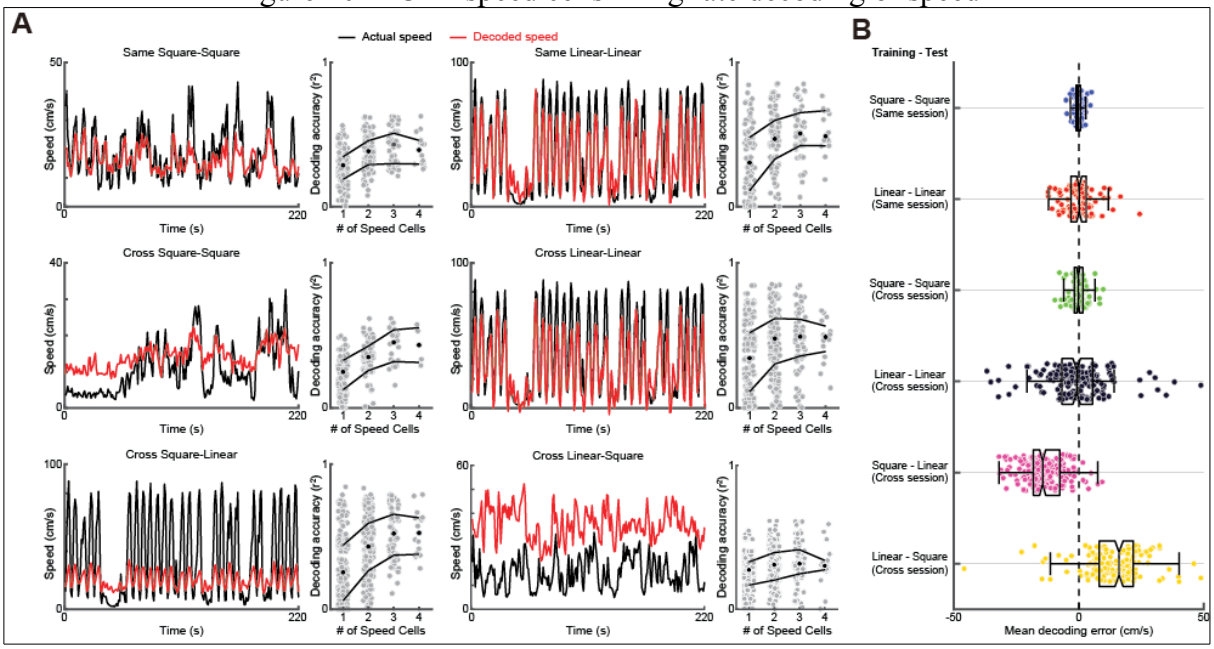


**Figure 10:** ***(A)*** On each column, the left panels show the time series of observed (gray) and decoded (red) speed from the firing rate of an individual CA1 speed cell. Linear decoders were trained using 350 seconds of data distinct from the 150-second testing period. Decoders were trained in one session and tested using either the same session ("Same") or another session ("Cross") recorded in the same day; the training and testing session arenas are stated in the title. The right panels show mean decoding accuracy for all possible models with the same fixed number of neurons within a session. Decoders were trained with 1 to 4 CA1 speed cells. Gray circles show individual sessions; black circles and lines show the median and 25-75% quartiles. ***(B)*** Boxplot of the mean difference between decoded and observed speeds for decoders trained with only one CA1 speed cell. Decoding error centered near zero when using training and test data from the same arena, and it was negative when the decoder was trained with data from the square arena and tested with linear track data; the opposite happened when using training and test data from the linear and square arenas, respectively, in which case the mean decoding error was positive. These results relate to the fact that animals achieved higher locomotion speeds in the linear track than in the square arena.

We next investigated for speed-correlated firing solemnly in the linear track. As in the square arena, we found that the majority (64%) of physiologically identified interneurons fulfilled the operational definition of speed cell in the linear track. However, we saw a different picture when analyzing the spiking activity of physiologically identified pyramidal cells. While their instantaneous firing rate did not correlate with speed in the square open-field arena (Figures 5, 6 and 7), 35% of the pyramidal cells exhibited speed-correlated firing in the linear track (Figure 11A,D). To gain insight into why some pyramidal cells would be considered speed cells only in the linear track but not in the open field, we next investigated their firing rate correlation with speed separately for left and right runs. The motivation for this is that most place cells have unidirectional place fields in the linear track, that is, they exhibit spatial-selective firing only when the animal runs in one of the directions (MCNAUGHTON; BARNES; O'KEEFE, 1983; MULLER et al., 1994).

Figure 11 – Pyramidal neurons place fields in the linear arena arise spurius speed score classification

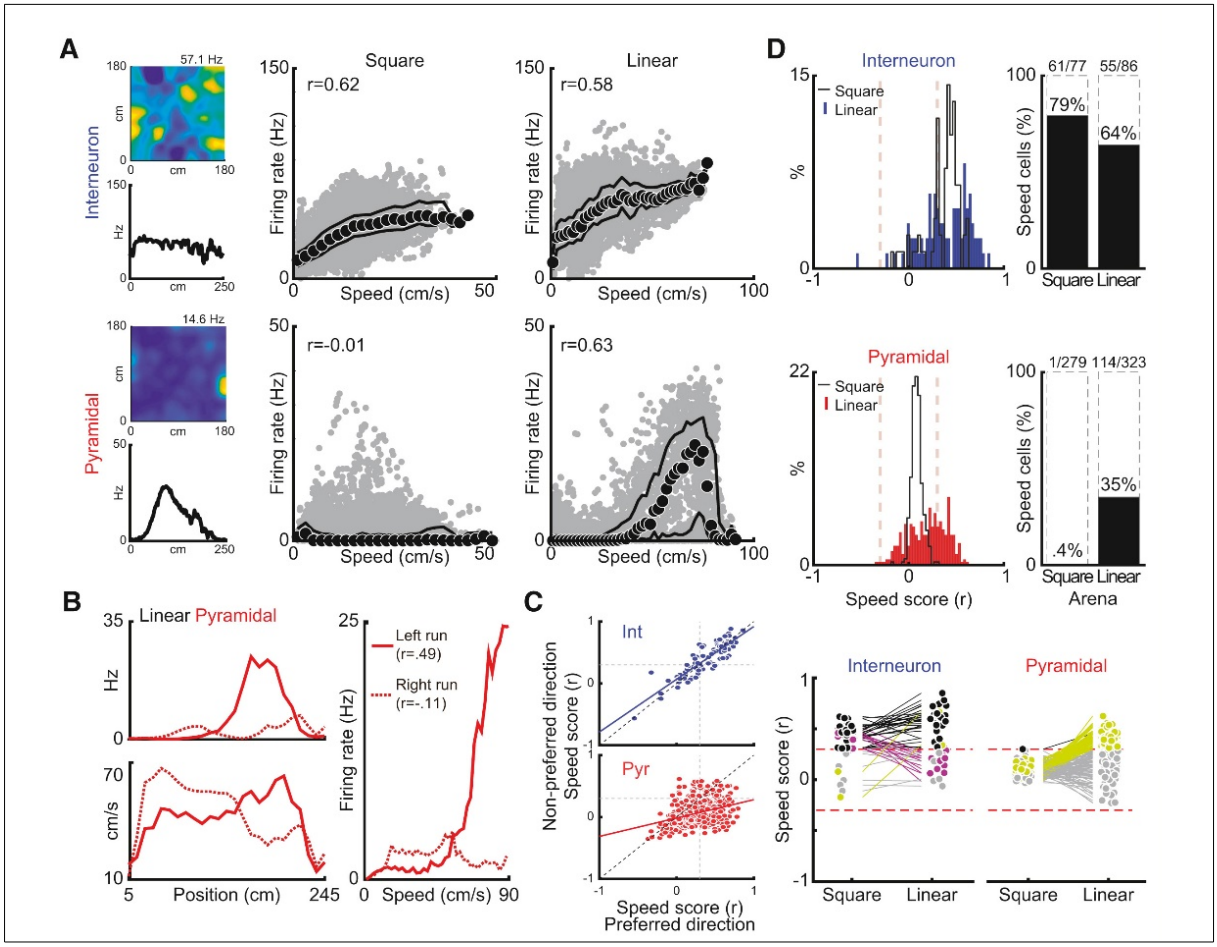


**Figure 11:** ***(A)*** Left panels show firing rate as a function of space in the square and linear arenas for an interneuron (top) and a pyramidal cell (bottom). Right panels show scatter plots of animal speed vs. firing rate for each arena and neuron type. Notice that the instantaneous firing rate of the interneuron correlates with speed in both arenas, while pyramidal cell activity is only correlated with speed in the linear track. ***(B)*** Left panels show mean locomotion speed (bottom) and mean firing rate for a pyramidal cell (top) during left and right runs in the linear track. Right panel shows the mean firing rate during left and right runs as functions of speed. ***(C)*** Scatter plots of speed scores during runs in the preferred (highest firing rate) and non-preferred directions shown separately for interneurons and pyramidal cells. Notice similar scores for interneurons for both run directions (slope: 0.85), while pyramidal cells have much higher speed scores for the preferred direction (slope: 0.29). ***(D)*** Distribution of speed scores and proportion of speed cells among interneurons and pyramidal cells in the square open-field arena ("Square") and in the linear track ("Linear"). Notice high percentage of speed cells among interneurons in both arenas, while around one-third of pyramidal cells are deemed speed cells only in the linear track.

Figure 11B shows a place cell that had a place field during leftward runs (top left panel); also shown is the average animal speed as a function of space for each running direction (bottom left panel). As expected from the nature of this task, the animal's speed stereotypically depended on space, being very low on the edges of the linear track where animals were rewarded, and high otherwise. We reasoned that the mutual dependence between speed and space in the linear track might lead to spurious correlations between speed and firing rate for place cells. By spurious we mean that these cells would not genuinely code for speed and the apparent correlation would be rather due to place fields at locations associated with high speeds. Consistent with this possibility, notice back in Figure 11A that

the example pyramidal cell spiked either at very high and very low rates during high speeds, which suggests run periods inside and outside the place field, respectively.

If the interdependence between speed and position accounts for the high speed scores observed for some pyramidal cells in the linear track (Figure 11D), the speed-correlated firing should follow spatial coding and be mostly unidirectional. On the other hand, if pyramidal cells truly code for speed, their speed-correlated firing should not depend on running direction (MCNAUGHTON; BARNES; O'KEEFE, 1983; MULLER et al., 1994). Our further analysis revealed evidence for the first possibility: notice in Figure 11B (right panel) that the average firing rate of the example place cell only increased with speed for the preferred running direction (defined as the direction of highest firing rate). At the group level, we found that pyramidal cells exhibited much higher speed scores for the preferred than the non-preferred direction (mean r preferred: 0.270±0.014, non-preferred: 0.065±0.012, $t(322)=13.5$, $p<10^{-32}$, paired t-test; Figure 11C bottom), and only 23% of the "speed cells" defined in the preferred direction were bidirectional. In stark contrast, the speed scores of interneurons did not depend on running direction (mean r preferred: 0.378±0.030, non-preferred: 0.388±0.028, $t(85)=-0.807$, $p=0.42$, paired t-test; Figure 11C, top), and 90% of the speed cells were bidirectional, a statistically significant higher proportion than for pyramidal cells ($\chi^2(1) = 72.94$, $p<0.00001$). Our results thus indicate that only interneurons code for speed in the linear track, and that the speed-correlated firing of pyramidal cells is spurious and due to the entanglement of speed and position in this task.

Our results thus indicate that only interneurons code for speed in the linear track, and that the speed-correlated firing of pyramidal cells is spurious and due to the entanglement of speed and position in this task. To further corroborate this conclusion, we next simulated computational models of speed and place cells using real behavioral data from linear and square arena sessions classified with speed score definition (Figures 12 to 14). In the simulations, the firing rate of the model place cells was solely determined by the instantaneous position of the animal, obtained from real data (Figure 11). Analogously, the firing rate of the model speed cells was solely determined by the instantaneous animal speed. As shown in Figure 13 and 14, simulation results were largely consistent with the conclusion reached above: (1) model speed cells had high speed scores in both open field and linear track simulations; (2) no model place cell correlated with speed in the open field but half of them were considered speed cells in the linear track, even though no speed coding was programmed for these cells.

Figure 12 – Computational model pipe line

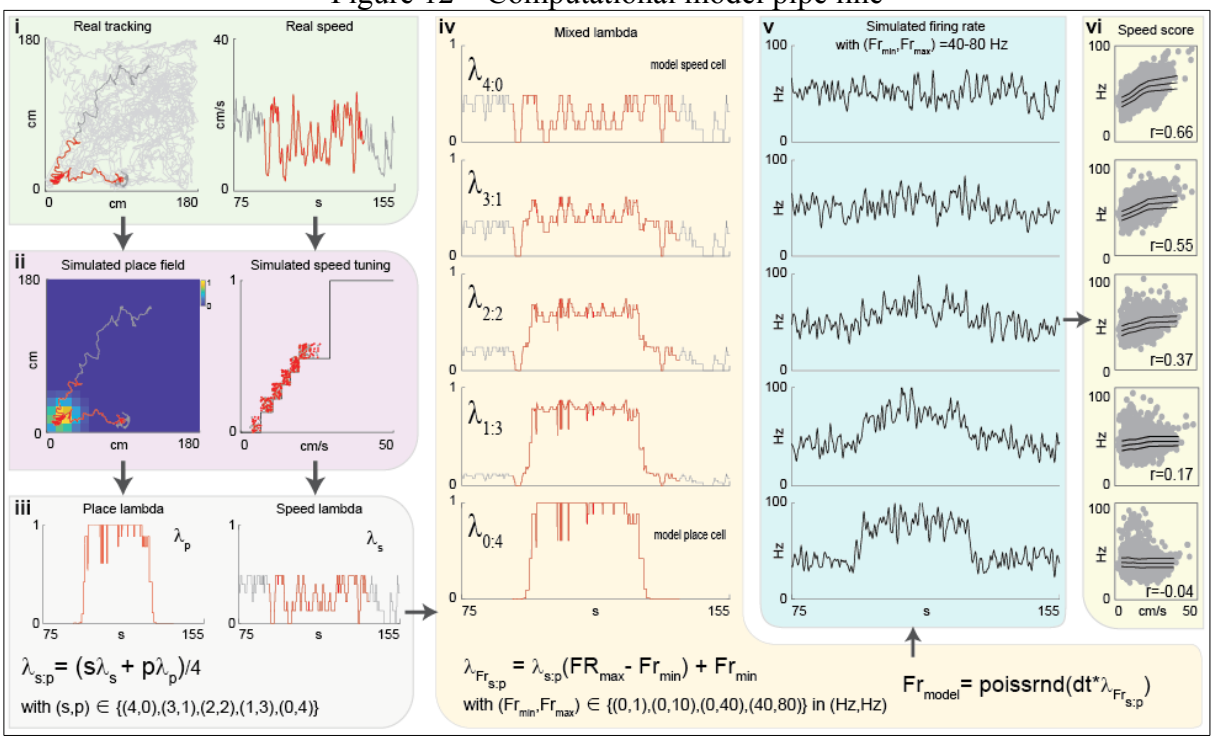


**Figure 12:** ***(i-vi)*** Computational models were implemented using the actual animal position and speed ***(i)***, which, based on simulated spatial and speed tuning curves ***(ii)***, determined the instantaneous values of the place ( $\lambda_p$ ) and speed ( $\lambda_s$ ) rate parameters ***(iii)***. We simulated five types of neuronal activity: model place or speed cells, which had firing rate solely determined by $\lambda_p$ or $\lambda_s$, respectively, as well as three mixed neuron types which had firing rate determined by a weighted sum of $\lambda_p$ and $\lambda_s$ ***(iv)***. The weighted rate parameters were normalized to be bounded between minimal and maximal values of choice. Finally, the instantaneous firing rate of the model cells was simulated as the outcome of a Poisson process ***(v)*** and used to compute the speed score *(vi)*.

Figure 13 – Computational models reveals speed score false positives in linear arena

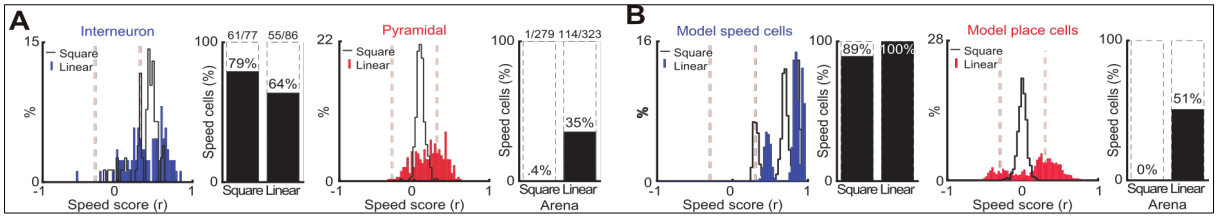


**Figure 13:** ***(A)*** Reproduction of figure 11D ***(B)*** Comparative classification of computational models with the speed score definition.

Figure 14 – Computational models speed score analysis details

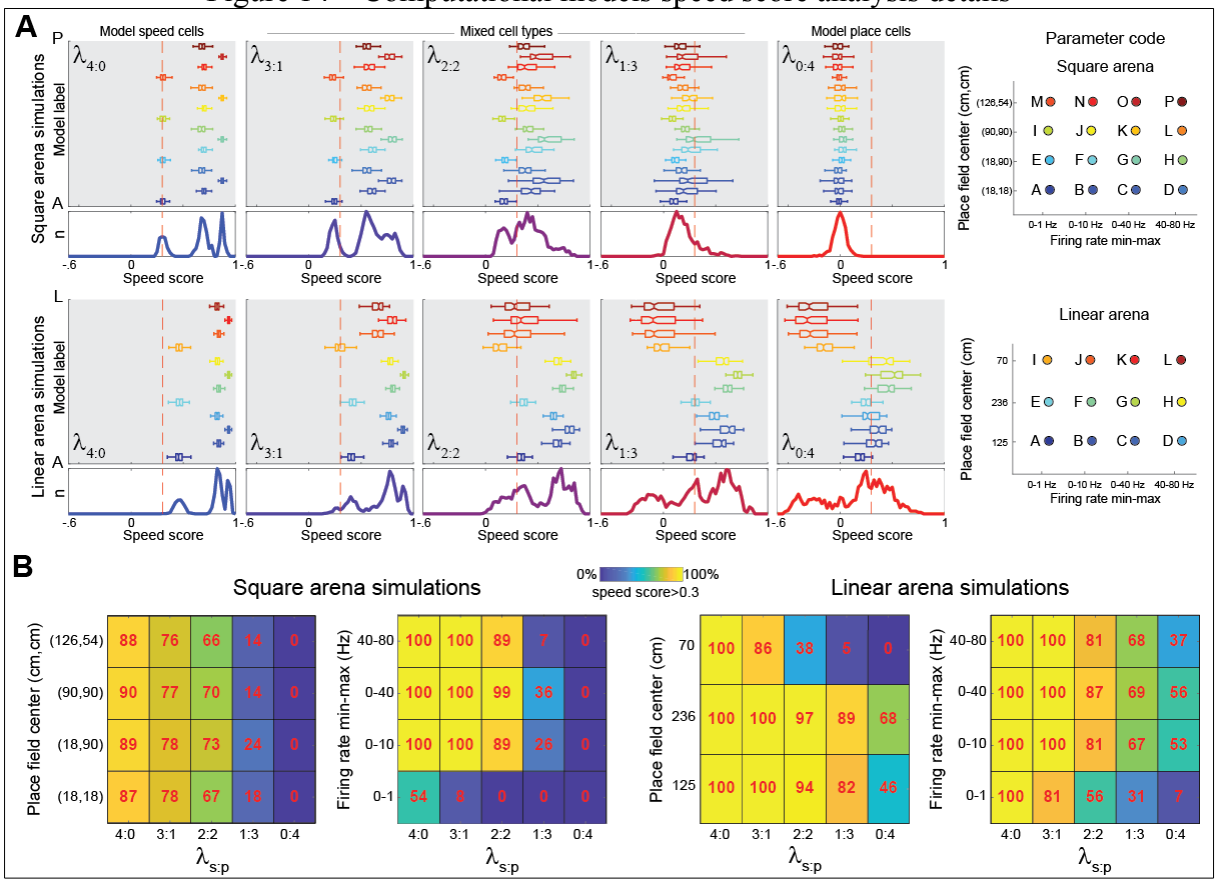


**Figure 14:** ***(A)*** Distribution of speed scores for model neurons simulated with different parameters (color/letter code on the right). Simulations were implemented using actual behavioral data (position and speed) from square open-field arena (top) or linear track (bottom) sessions. The different columns show results for model neurons with different levels of speed and place coding, from pure speed cells ( $\lambda_{4:0}$ ) to pure place cells ( $\lambda_{0:4}$ ) (see Figure 12). ***(B)*** Percentage of model neurons considered speed cells by the operational definition (speed score>0.3). In each panel, the leftmost and rightmost columns show results for pure speed and place cells, respectively. Notice in the linear track that a high percentage of pure place cells ( $\lambda_{0:4}$ ) are deemed speed cells even though no speed coding was simulated for these cells.

## 3.7. SPEED CELL CLASSIFICATION BASED ON LINEAR NON-LINEAR MODELS

Finally, we employed a recently described statistical model-based approach (HARDCASTLE et al., 2017) to infer speed and positional coding by interneurons and pyramidal cells in each arena. Under this framework, the spike train is modeled as a Poisson process of either fixed mean or variable mean dependent on the instantaneous speed and/or position of the animal. In the latter case, the mean rate of the Poisson process is set as the exponential of a linear combination of speed and positional variables (see Method Details), hence these models have been referred to linear-nonlinear-Poisson (LN) models (HARDCASTLE et al., 2017). Different LN models are used to fit the spiking activity of real neurons, whose coding properties can then be inferred by comparing the log-likelihood increase (LLHi) in relation to a Poisson model of fixed firing rate and predictive performance across models (HARDCASTLE et al., 2017).

We first validated the utility of the LN model approach using simulations of speed and place cell models. Cells were considered to have no coding preference when the LLHi's for LN position models and LN speed models were not statistically significantly higher than 0. Otherwise, cells were classified according to the magnitude and significance of the LLHi's. As expected, the firing rate of simulated speed cells was better predicted by LN speed models – that is, statistical models whose Poisson rate takes into account the instantaneous speed of the animal (Figure 15). Conversely, simulated place cells were better predicted by LN position models, irrespective of the arena (Figure 15). When applying this statistical approach to real spiking data, most interneurons had higher LLHi for LN speed models in both the square arena (71%) and linear track (75%), and only 10-15% displayed higher LLHi for LN position models; 9-18% were not significantly modulated by position or speed. In stark contrast, the vast majority of pyramidal cells had higher LLHi for LN position models in both the square arena (94%) and linear track (88%), while just 6% in either arena did not display coding preference. No pyramidal cell had higher LLHi for LN speed models in the square arena, and only 6% in the linear track. Taking into account all cells irrespective of the significance of the LLHi's, in both arenas the percentage of cells whose firing rate was better predicted by speed was high for interneurons (73%) and low for pyramidal cells (0-9%) (Figure 16). In all, this model-based statistical approach reveals a preferential encoding of speed by interneurons and of space by pyramidal cells, thus consistent with the conclusions reached above through the analysis of correlation coefficients. Therefore, the final result of this thesis is that the speed score is not a valid metric to evaluate the presence of locomotion speed coding in neuronal activity. Co-variants (i.e. position) can introduce unexpected

influence, these can be solved with a multivariate approach such as the suggested linear-non-linear model prediction accuracy ($r^2$) difference ratio (Figure 17).

Figure 15 – LN models overcome false positives of speed score in simulated cells

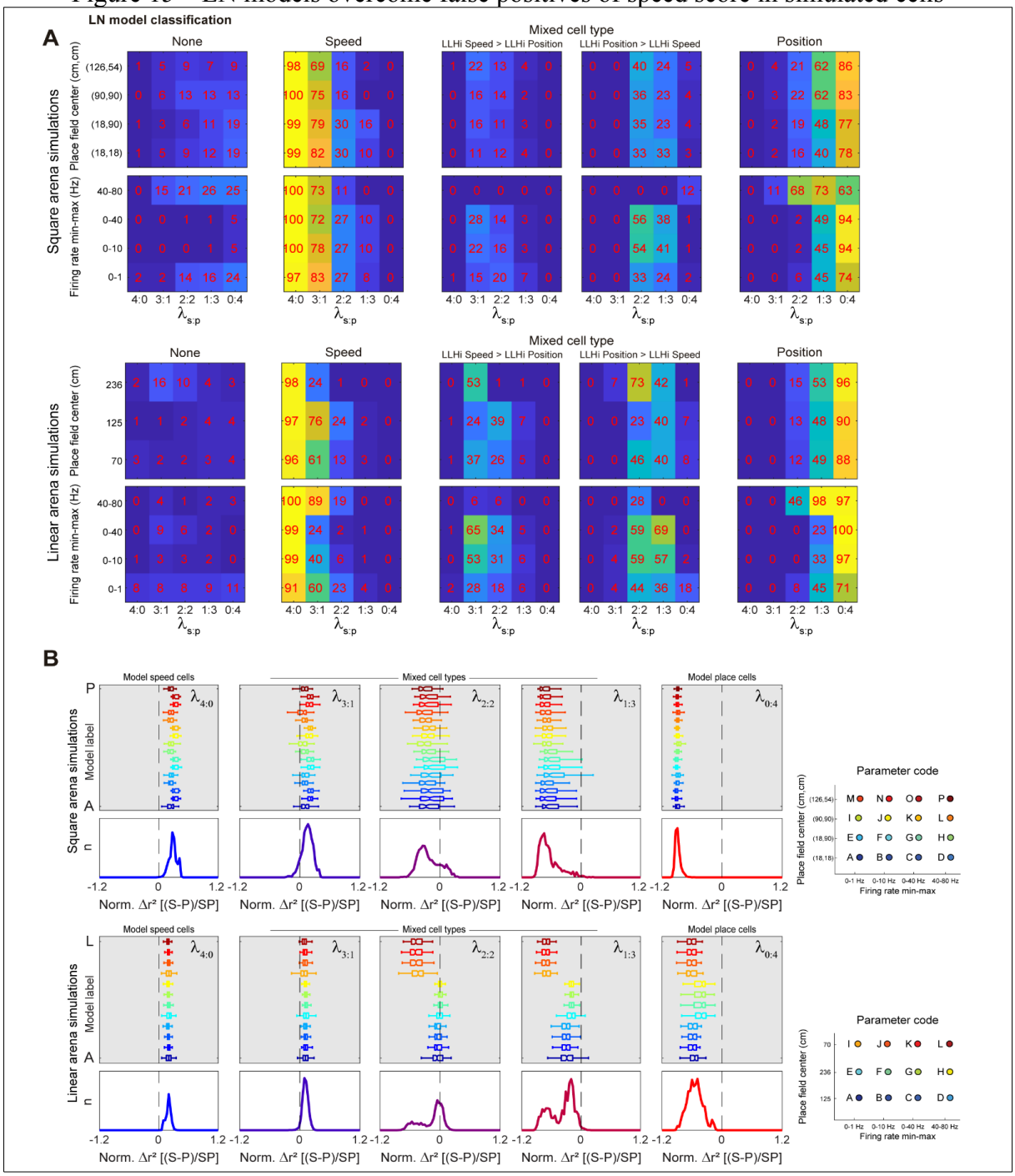


**Figure 15:** ***(A)*** Simulations of place and speed cells were performed as in Figures 13-15. Linear-nonlinear-Poisson (LN) models were used to classify coding properties of the simulated neurons (see Method Details and Hardcastle et al., 2017). Cells were classified as having no coding preference ("None") when the log-likelihood increase (LLHi) for LN speed models and LN position models in relation to a Poisson model of fixed firing rate was not significantly higher than 0. Otherwise, cells were classified as "Speed" or "Position" depending on the significance of the corresponding LLHi. The "Mixed cell type" classification denotes cells whose LLHi of LN speed & position models was statistically significantly higher than the LLHi of isolated LN position or LN speed models. Notice that most of pure speed cells ( $\lambda_{4:0}$ ) and pure place cells ( $\lambda_{0:4}$ ) were correctly classified as such in either arena. ***(B)*** Normalized difference in firing rate prediction accuracy ($\Delta r^2$) between speed and position LN models (as in Figure 16E) for simulations in the square and linear arenas (as in Figure 15). Positive values denote better prediction by speed, and negative values, by position.

Figure 16 – LN models corroborate preferential encoding of speed by interneurons and of space by pyramidal cells in real data

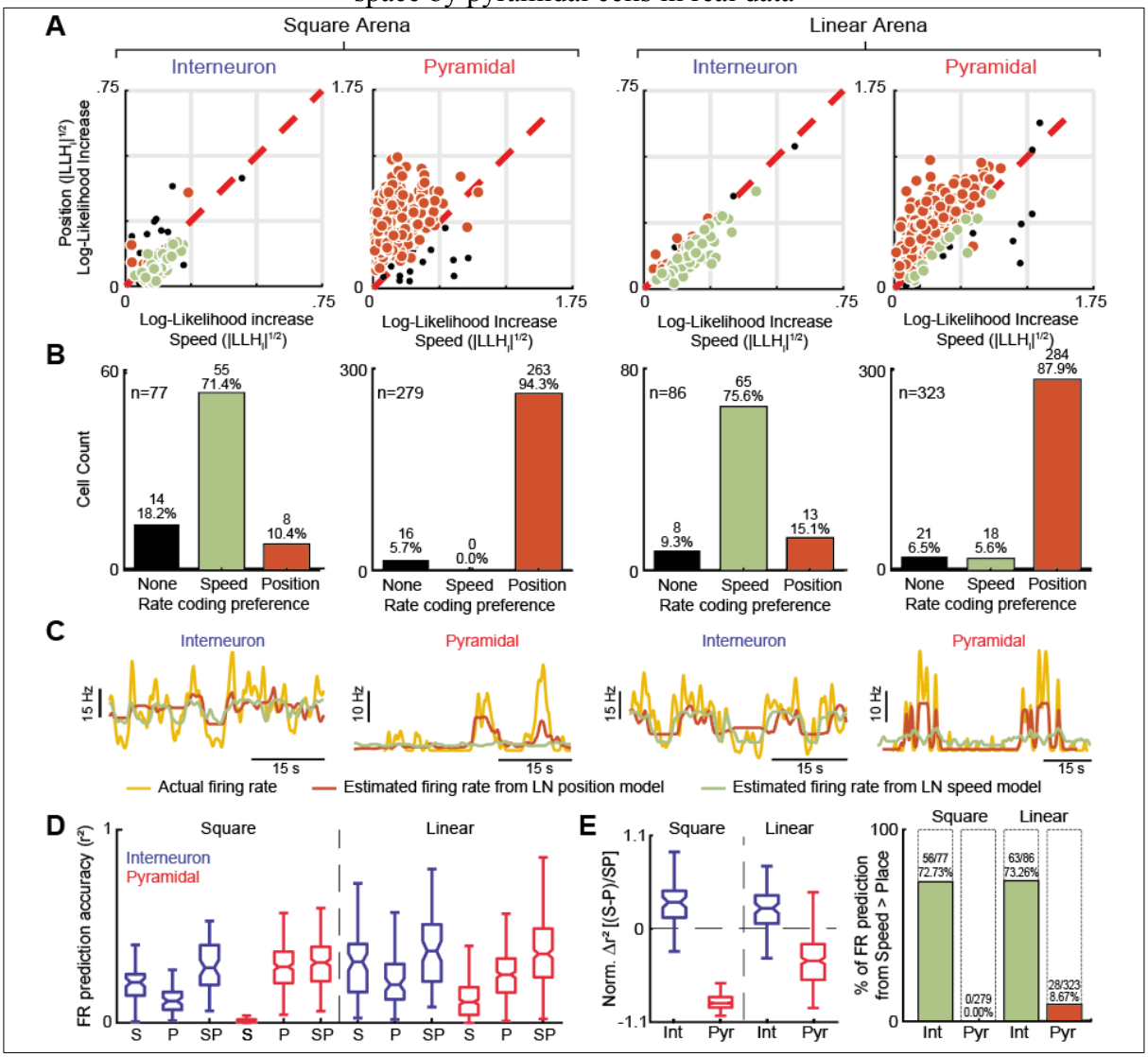


**Figure 16: (A)** Scatter plots of the log-likelihood increase ($LLH_i$) for LN firing rate models considering position (y-axis) or speed (x-axis) in comparison to a fixed mean firing rate model. Results plotted separately for each arena and cell type, as labeled. Green and orange circles denote cells whose firing rate was better explained by speed or position, respectively; black circles show cells without statistically significant influence of either variable. **(B)** Percentage of cells preferentially modulated by speed (green) or position (orange), as defined by the highest significant $LLH_i$. The percentage of non-modulated cells (non-significant $LLH_i$) is also shown (black). **(C)** Examples of firing rate time series plotted along with the predicted firing rate time series from LN models based on the instantaneous position or speed. Notice that the pyramidal cell firing rate is not well fitted by the LN speed model in either arena. **(D)** Prediction accuracy for LN models based on speed (S), position (P) or both variables (SP), defined as the coefficient of determination ($r^2$) between the predicted and the actual firing rate (FR) time series. **(E)** (Left) Normalized difference in FR prediction accuracy ($\Delta r^2$) between speed and position LN models. Positive values denote better prediction by speed, and negative values, by position. (Right) Percentage of cells whose FR was better predicted by speed than position.

Figure 17 – LN models and speed score classification confusion matrices

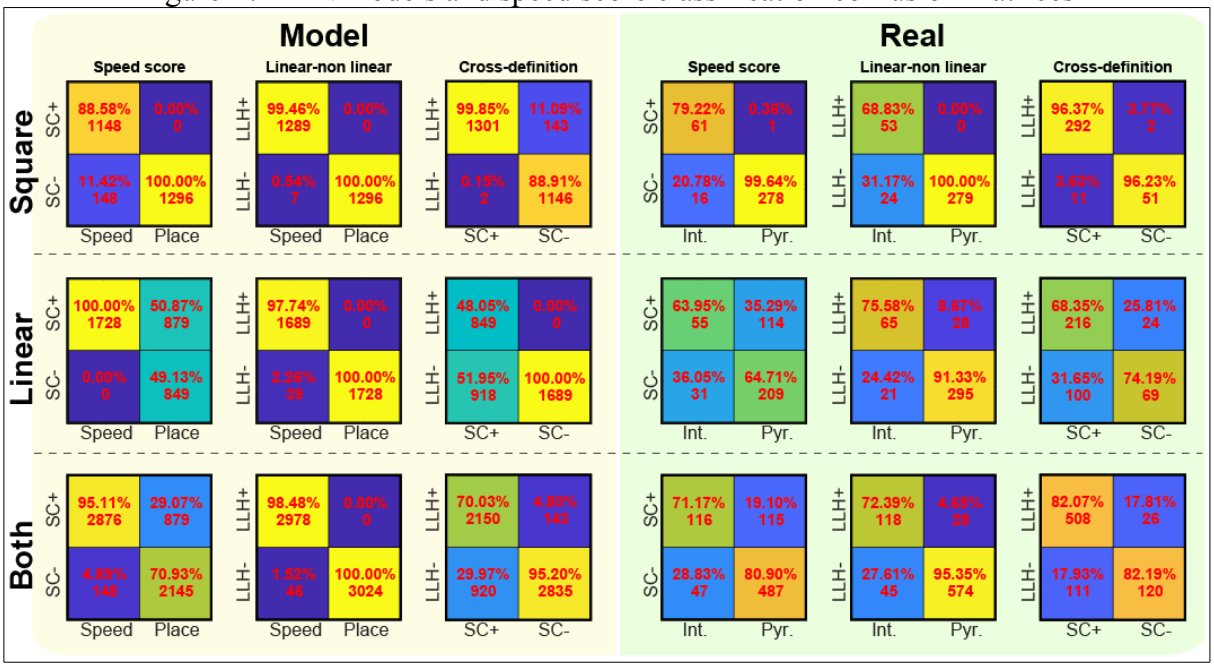


**Figure 17:** ***(Left)*** Percentage of toy models of speed and place cells that were classified as speed cells by the standard speed score (SC) definition or by the log-likelihood increase (LLHi) of linear-nonlinear (LN) speed models. SC+ denotes cells whose absolute correlation coefficient between firing rate and speed was >0.3; LLH+ denotes cells whose LLHi for LN speed models was statistically significantly higher than 0 and higher than the LLHi of LN position models. ***(Right)*** Panels show the same but for real interneurons and pyramidal cells.

# 4 DISCUSSION

To the best of our knowledge, we have here performed the most thorough neuroelectrophysilogical analysis of speed-correlated firing rate in the dorsal hippocampus to date. Our results show that a subpopulation of hippocampal neurons has firing rate highly correlated with speed at the sub-second timescale. In line with recent work (KROPFF et al., 2015), we referred to these neurons as "speed cells". We found that the speed-correlated firing of CA1 speed cells occurs in two different contexts, and irrespective of exact position in space and elapsed time. Moreover, the firing rate changes of speed cells tended to follow, more than lead, the changes in locomotion speed. Perhaps of most importance for network models of navigation, our results indicate that the subpopulation of CA1 speed cells is exclusively comprised of inhibitory interneurons. This central conclusion was achieved because (1) virtually no pyramidal cell correlated with speed in the open field arena, and (2) the speed-correlated firing of some pyramidal cells in the linear track could be accounted for by spatial coding along with the mutual dependence of animal position and speed in this arena.

## 4.1. PYRAMIDAL CELLS UNEXPECTED RESULTS

At first glance, our main conclusion may seem at odds with numerous reports of firing rate correlations with speed by both pyramidal cells and interneurons (MCNAUGHTON; BARNES; O'KEEFE, 1983; WIENER; PAUL; EICHENBAUM, 1989; O'KEEFE et al., 1998; ZHANG et al., 1998; CZURKÓ et al., 1999, 2011; HIRASE et al., 1999; EKSTROM et al., 2001; NITZ; MCNAUGHTON, 2004; MAURER et al., 2005). A main methodological difference, however, is that we have explored for firing rate correlations with speed at the sub-second scale in which changes in locomotion occur, while previous studies have mostly focused on the average firing rate. Here we were able to reproduce the finding that the average firing rate of both pyramidal cells and interneurons is modulated by speed, even in the open field (Figure 7). However, the speed correlation of the instantaneous firing rate of pyramidal cells was much weaker than that of interneurons, and speed in the open field could only be reliably decoded from interneurons (Figure 7). In the linear track, we saw a different picture in which the firing rate of 35% of pyramidal cells correlated with speed, but further analysis showed that such correlation could be explained on other grounds than speed coding (Figure 11).

## 4.2. SPEED CELLS DEFINITION

Indeed, when first analyzing the results, it called our attention that the apparent speed coding by pyramidal cells would occur just in one type of arena (linear track) but not the other (open field) and would depend on running direction (Figure 11). This led us to conclude that it was more parsimonious to ascribe such speed-correlated firing to a by-product of place coding along with the fact that speed and position could not be disentangled with speed score in the linear track due to the nature of the task, which required animals to run back and forth between the end goals. For instance, place cells with place fields in the middle of the track, where the animals display highest speeds in this task, will be considered speed cells by the speed score definition. Consistent with this, computer simulations using the actual behavior of the animal showed that the firing rate of emulated place cells with no programmed speed coding also correlates with speed in the linear track, but not in the open field (Figure 13 and 14). This comproved that Pearson's coefficient (speed score) is not the appropriate metric to evaluate the speed coding in neurons. The measured variables ethological interdependence together with conjuctive coding are some aspects that imposes the necessity for a multivariate approach to evaluate coding. Statistical LN models is the analysis framework that we chose to solve such multivariate issue; applying into simulations it overcame the false positives classification in the linear arena. In real data, statistical LN models corroborated that the vast majority of pyramidal cells preferentially encoded position in the linear track, and not speed, with the opposite happening for interneurons (Figure 16).

Although neuronal activity correlated with speed had been previously reported in the medial entorhinal cortex (SARGOLINI et al., 2006; WILLS; BARRY; CACUCCI, 2012), speed coding in the hippocampal-entorhinal system has only more recently been better characterized (KROPFF et al., 2015; HINMAN et al., 2016; PÉREZ-ESCOBAR et al., 2016; YE et al., 2018). Namely, Kropff et al. (2015) showed that the medial entorhinal cortex has neurons whose firing rate linearly correlates with speed and called them "speed cells", a nomenclature also adopted here (see below for discussion). They further showed that these neurons differed from grid and head direction cells, suggesting a functionally dedicated group (HARDCASTLE et al., 2017), and that they were stable across contexts. Relevantly, Kropff et al. (2015) have also reported cells with similar characteristics in the hippocampus. Further consistent with our results, in a recent follow-up study, the same group reported that a large proportion of entorhinal cortex speed cells are fast-spiking interneurons (PÉREZ-ESCOBAR et al., 2016; YE et al., 2018). Moreover, they showed that a subset of speed-modulated GABAergic neurons projects directly to the hippocampus (YE et al., 2018). Interestingly, a main difference between the two regions is that the hippocampal speed cells better correlate

with immediate past speeds (-65 ms, Figure 6; see also Kropff et al., 2015), while speed cells in the entorhinal cortex display prospective coding – that is, their firing rate correlates better with immediate future speeds (+60 ms, KROPFF et al., 2015). These findings, however, should be interpreted with care since the video frames were acquired with a temporal resolution of 33-20 ms (30-50 Hz). However, the persistence of the codification of a same variable in past and future can have computational implications to the neural network. We hypothesize that the neural network can compare such signals to provide either time itself or a derivative of the recorded variable in time – acceleration in this case.

It is worth noticing that we have used a much more conservative threshold for defining speed cells ($|r|>0.3$) than the one based on surrogate data used in recent studies (KROPFF et al., 2015; PÉREZ-ESCOBAR et al., 2016; YE et al., 2018). This more stringent threshold was motivated by the verification of a clear bimodal distribution of speed scores, which would not be well separated by the surrogate-based threshold (Figure 3). Moreover, excitatory cells of the entorhinal-hippocampal system have weak but positive correlations with speed (YE et al., 2018), likely because they are most active during traversals of their spatial receptive field, thus causing a positive bias for higher activity during locomotion. We believe the use of less conservative thresholds may account for the inclusion of excitatory cells in the population of speed cells in the entorhinal cortex studies (KROPFF et al., 2015; PÉREZ-ESCOBAR et al., 2016; YE et al., 2018).

### 4.3. DISCLAIMER OF NOMECLATURE AND JARGONS

The definition of neuronal encoding is often linked to the capacity of decoding information from neuronal activity (i.e., to neuronal decoding). That is, in practice, a neuron is considered to encode information about a given feature if it is possible to retrieve this information from the analysis of its spike train (BIALEK et al., 1991; RIEKE, 1999; QUIAN QUIROGA; PANZERI, 2009; ROLLS; TREVES, 2011; STANLEY, 2013). In this sense, the present work employed the same operational definition as in most of the current neuroscience research: since animal speed could be successfully decoded from the firing rate of hippocampal speed cells, these cells were interpreted as encoding information about speed. However, it may be too simplistic to assume that a value-encoding process takes place solely based on correlations between external variables and neuronal activity (WIENER; PAUL; EICHENBAUM, 1989). Instead of encoding the scalar value of speed, the hippocampal interneurons may be rather only modulated by speed. Judging whether information is value-encoded also depends on knowing how such a code – if existent – is read by downstream neurons, a challenging and seldom tackled question in neuroscience (BUZSÁKI, 2010;

STANLEY, 2013). Thus, as long as neuronal coding and decoding are dual definitions, it is impossible to operationally separate encoding from modulated activity, and the natural question as to whether inhibitory interneurons provide an actual speed signal is at present difficult to solve. In any case, it is clear that speed does affect local networks through the activity of interneurons.

We also note that the nomenclature employed here and in other recent studies – namely of calling neurons whose instantaneous firing rate has high correlation with speed as "speed cells" – may not be the most appropriate one. We opted to use this notation for the sake of convenience; clearly, "speed cells" reads much faster than "neurons whose firing rate correlates with speed". But aside from the convenience of notation, we do not mean to imply that "speed cells" only code (if they code) for speed. For instance, we here showed that hippocampal speed cells are interneurons, and, in fact, speed modulates a large proportion of local GABAergic cells (Figure 5). Inhibitory interneurons are well known to have several functions, such as control of input and output activity of pyramidal cells, generation of oscillatory activity and segregation of cell assembly sequences (FREUND; BUZSÁKI, 1996; KLAUSBERGER; SOMOGYI, 2008; PELKEY et al., 2017). Thus, the "speed cells" certainly play many more roles in addition to conveying speed-modulated inhibition to the local network. Of note, similar terminology has been previously employed for other types of neurons, to start with "place cells" which are known to code other variables rather only position (EICHENBAUM, 2000; WOOD et al., 2000, p. 200; ARONOV; NEVERS; TANK, 2017).

## 4.4. COMPARTIVE RESULTS

Neurons of the hippocampal formation have been previously linked to both allocentric- and egocentric-based spatial navigation (MOSER; KROPFF; MOSER, 2008; BUZSÁKI; MOSER, 2013; HARTLEY TOM et al., 2014). Theoretically, path integration can be achieved from the knowledge of the initial position, locomotion direction and traveled distance (MCNAUGHTON et al., 2006). To estimate the latter, speed must be integrated over elapsed time. Accordingly, models of path integration assume the existence of a speed signal impinging on specific neurons (FUHS; TOURETZKY, 2006; MCNAUGHTON et al., 2006; BURAK; FIETE, 2009; NAVRATILOVA et al., 2012; COUEY et al., 2013). While the sparse spiking of pyramidal cells would make them well suited for position coding, the high firing rates of GABAergic interneurons may be instantaneously adjusted according to speed and would thus provide the required signal to the network. Interestingly, we found that speed cells decode speed better than pyramidal cells even after controlling for differences in firing

rate (Figure 7E), likely because interneurons tend to be active all over the arena. Of note, the CA1 speed cells were not modulated by movement direction (not shown). Therefore, for speed cells to play a role in path integration, the speed information conveyed by them should be combined with the directional information provided by head-direction cells. Under this scenario, path integration would not be a function of a unique cell type but would require downstream reader neurons to integrate multiple sources of information.

Our results are consistent with a recent computational model of phase precession (CHADWICK; VAN ROSSUM; NOLAN, 2016). This model was able to account for the speed dependence of the rate of change in the spiking theta phase of place cells as the animal traverses the place field, in which the temporal slope of phase precession is steeper for faster speeds. In turn, the variable temporal slope allows for a fixed relation between spiking theta phase and position at different running speeds (HUXTER; BURGESS; O'KEEFE, 2003; GEISLER et al., 2007, p. 20). The model results crucially relied on the activity of interneurons, which were predicted to receive excitatory inputs dependent on speed (CHADWICK; VAN ROSSUM; NOLAN, 2016). Consistent with this possibility, glutamatergic cells of the medial septum were recently shown to provide CA1 interneurons with a depolarizing drive that increases with running speed (FUHRMANN et al., 2015). Neurons modulated by speed in other subcortical structures such as the mammillary bodies, habenula, and interpeduncular nucleus could potentially contribute (SHARP; TURNER-WILLIAMS, 2005; SHARP; TURNER-WILLIAMS; TUTTLE, 2006). Regardless of the source of excitation, by demonstrating their high modulation by speed, our results support the idea that the activity of inhibitory interneurons in CA1 would allow for flexible timescales of theta spiking sequences (CHADWICK; VAN ROSSUM; NOLAN, 2016).

On average, pyramidal cells spiked more with running speed (Figure 7A and B). This result is seemingly discrepant with the positive speed correlation exhibited by most speed cells (Figures 3 and 5), which are interneurons and should thus inhibit pyramidal cells at higher speeds. Possible solutions to this conundrum include network scenarios in which (1) both interneurons and pyramidal cells receive a common, speed-dependent excitatory drive; or in which (2) the firing rate of interneurons is primarily determined by the activity of pyramidal cells at the population level (which would provide a higher net excitation with higher speeds); or in which (3) synaptic connections among inhibitory interneurons lead to a disinhibition of pyramidal cells. Evidence for the latter scenario has been reported by Fuhrmann et al. (2015), who showed that interneurons located in stratum oriens/alveus such as OLM cells are excited by septal glutamatergic neurons and in turn inhibit interneurons in stratum radiatum and stratum lacunosum-moleculare that mediate feedforward inhibition onto pyramidal cells. However, the recordings analyzed here targeted the pyramidal cell layer, and

it is thus likely that the speed cells also comprised fast-spiking, parvalbumin-positive basket cells that provide perisomatic inhibition. Actually, since a high percentage of interneurons were classified as speed cells (Figures 5, 6, 11, 14 and 16), we believe the CA1 speed cell population included multiple interneuron subtypes.

Our findings are also consistent with a recent study in awake head-fixed mice that tracked neuronal activity through $Ca^{+2}$ imaging (ARRIAGA; HAN, 2017). They found that $Ca^{+2}$ fluctuations of most interneurons (>74%) were positively correlated with speed while the animals navigated in a virtual environment, and that speed modulated both parvalbumin- and somatostatin-positive interneurons located in different hippocampal layers, which is to say that speed modulated different morphological subtypes of interneurons. Interestingly, the fluorescence signals were anti-correlated with speed for ~14-18% of cells (ARRIAGA; HAN, 2017) , a higher percentage than the 8.6% of "negative" speed cells found here (8/93, Figure 3). Also similar to our findings, the imaging results showed that the speed correlations of $Ca^{+2}$ fluctuations were stable over time and different virtual environments.

In summary, we have shown that inhibitory interneurons, and not pyramidal cells, are likely to convey a reliable rate-coded speed signal to the hippocampus, which is stable across contexts, position in space and elapsed time. This finding should shed new light on network models of spatial navigation.

## 5 REFERENCE


ARONOV, D.; NEVERS, R.; TANK, D. W. Mapping of a non-spatial dimension by the hippocampal–entorhinal circuit. **Nature**, v.543, n.7647, p. 719-722, 1 mar. 2017. Available at <https://doi.org/10.1038/nature21692>. Accessed on: 21 aug. 2019.

ARRIAGA, M.; HAN, E. B. Dedicated Hippocampal Inhibitory Networks for Locomotion and Immobility. **Journal of Neuroscience**, v.37, n.38, p. 9222-9238, 20 sep. 2017. Available at <https://doi.org/10.1523/JNEUROSCI.1076-17.2017>. Accessed on: 21 aug. 2019.

BIALEK, W. et al. Reading a neural code. **Science**, v.252, n.5014, p. 1854-1857, 28 jun. 1991. Available at <https://doi.org/10.1126/science.2063199>. Accessed on: 21 aug. 2019.

BLUMBERG, M. S. The developmental origins of spatial navigation: Are we headed in the right direction?. **Trends in Neurosciences**, v.38, n.2, p. 67-68, 1 feb. 2015. Available at <https://doi.org/10.1016/j.tins.2015.01.001>. Accessed on: 23 aug. 2019.

BUCKNER, R. L. The Role of the Hippocampus in Prediction and Imagination. **Annual Review of Psychology**, v.61, n.1, p. 27-48, 1 jan. 2010. Available at <https://doi.org/10.1146/annurev.psych.60.110707.163508>. Accessed on: 6 dec. 2019.

BURAK, Y.; FIETE, I. R. Accurate Path Integration in Continuous Attractor Network Models of Grid Cells. **PLOS Computational Biology**, v.5, n.2, p. e1000291, 20 feb. 2009. Available at <https://doi.org/10.1371/journal.pcbi.1000291>. Accessed on: 21 aug. 2019.

BUZSÁKI, G. Neural Syntax: Cell Assemblies, Synapsembles, and Readers. **Neuron**, v.68, n.3, p. 362-385, 4 nov. 2010. Available at <https://doi.org/10.1016/j.neuron.2010.09.023>. Accessed on: 21 aug. 2019.

BUZSÁKI, G. Theta Oscillations in the Hippocampus. **Neuron**, v.33, n.3, p. 325-340, 31 jan. 2002. Available at <https://doi.org/10.1016/S0896-6273(02)00586-X>. Accessed on: 21 aug. 2019.

BUZSÁKI, G. Theta rhythm of navigation: Link between path integration and landmark navigation, episodic and semantic memory. **Hippocampus**, v.15, n.7, p. 827-840, 1 jan. 2005. Available at <https://doi.org/10.1002/hipo.20113>. Accessed on: 19 feb. 2020.

BUZSÁKI, G.; MOSER, E. I. Memory, navigation and theta rhythm in the hippocampal-entorhinal system. Nature Neuroscience, v.16, n.2, p. 130-138, 1 feb. 2013. Available at <https://doi.org/10.1038/nn.3304>. Accessed on: 21 aug. 2019.

CHADWICK, A.; VAN R. M. C.; NOLAN, M. F. Flexible theta sequence compression mediated via phase precessing interneurons. **eLife**, v.5, p. e20349, 8 dec. 2016. Available at <https://doi.org/10.7554/eLife.20349.001>. Accessed on: 6 dec. 2019.

COUEY, J. J. et al. Recurrent inhibitory circuitry as a mechanism for grid formation. **Nature Neuroscience**, v.16, n.3, p. 318-324, 1 mar. 2013. Available at <https://doi.org/10.1038/nn.3310>. Accessed on: 21 aug. 2019.

CSICSVARI, J. et al. Oscillatory Coupling of Hippocampal Pyramidal Cells and Interneurons in the Behaving Rat. **Journal of Neuroscience**, v.19, n.1, p. 274-287, 1 jan. 1999. Available at <https://doi.org/10.1523/JNEUROSCI.19-01-00274.1999>. Accessed on: 21 aug. 2019.

CZURKÓ, A. et al. Sustained activation of hippocampal pyramidal cells by 'space clamping' in a running wheel: Sustained discharge of hippocampal pyramidal cells. **European Journal of Neuroscience**, v.11, n.1, p. 344-352, 1 jan. 1999. Available at <https://doi.org/10.1046/j.1460-9568.1999.00446.x>. Accessed on: 6 dec. 2019.

CZURKÓ, A. et al. Theta Phase Classification of Interneurons in the Hippocampal Formation of Freely Moving Rats. **Journal of Neuroscience**, v.31, n.8, p. 2938-2947, 23 feb. 2011. Available at <https://doi.org/10.1523/JNEUROSCI.5037-10.2011>. Accessed on: 21 aug. 2019.

DIBA, K.; BUZSÁKI, G. Hippocampal Network Dynamics Constrain the Time Lag between Pyramidal Cells across Modified Environments. **Journal of Neuroscience**, v.28, n.50, p. 13448-13456, 10 dec. 2008. Available at <https://doi.org/10.1523/JNEUROSCI.3824-08.2008>. Accessed on: 21 aug. 2019.

DRAGOI, G.; BUZSÁKI, G. Temporal Encoding of Place Sequences by Hippocampal Cell Assemblies. **Neuron**, v.50, n.1, p. 145-157, 1 apr. 2006. Available at <https://doi.org/10.1016/j.neuron.2006.02.023>. Accessed on: 6 dec. 2019.

EICHENBAUM, H. Hippocampus: Mapping or memory?. **Current Biology**, v.10, n.21, p. R785-R787, 1 nov. 2000. Available at <https://doi.org/10.1016/S0960-9822(00)00763-6>. Accessed on: 21 aug. 2019.

EKSTROM, A. et al. NMDA Receptor Antagonism Blocks Experience-Dependent Expansion of Hippocampal "Place Fields". **Neuron**, v.31, n.4, p. 631-638, 1 aug. 2001. Available at <https://doi.org/10.1016/S0896-6273(01)00401-9>. Accessed on: 6 dec. 2019.

FERBINTEANU, J.; SHAPIRO, M. L. Prospective and Retrospective Memory Coding in the Hippocampus. **Neuron**, v.40, n.6, p. 1227-1239, 1 dec. 2003. Available at <https://doi.org/10.1016/S0896-6273(03)00752-9>. Accessed on: 6 dec. 2019.

FRANK, L. M.; BROWN, E. N.; WILSON, M. A. A Comparison of the Firing Properties of Putative Excitatory and Inhibitory Neurons From CA1 and the Entorhinal Cortex. **Journal of Neurophysiology**, v.86, n.4, p. 2029-2040, 1 oct. 2001. Available at <https://doi.org/10.1152/jn.2001.86.4.2029>. Accessed on: 6 dec. 2019.

FREUND, T.; BUZSÁKI, G. Interneurons of the hippocampus. **Hippocampus**, v.6, n.4, p. 347-470, 1 jan. 1996. Available at <https://doi.org/10.1002/(SICI)1098-1063(1996)6:4<347::AID-HIPO1>3.0.CO;2-I>. Accessed on: 21 aug. 2019.

FUHRMANN, F. et al. Locomotion, Theta Oscillations, and the Speed-Correlated Firing of Hippocampal Neurons Are Controlled by a Medial Septal Glutamatergic Circuit. **Neuron**, v.86, n.5, p. 1253-1264, 1 jun. 2015. Available at <https://doi.org/10.1016/j.neuron.2015.05.001>. Accessed on: 6 dec. 2019.

FUHS, M. C.; TOURETZKY, D. S. A Spin Glass Model of Path Integration in Rat Medial Entorhinal Cortex. **Journal of Neuroscience**, v.26, n.16, p. 4266-4276, 19 apr. 2006. Available at <https://doi.org/10.1523/JNEUROSCI.4353-05.2006>. Accessed on: 21 aug. 2019.

FUJISAWA, S. et al. Behavior-dependent short-term assembly dynamics in the medial prefrontal cortex. **Nature Neuroscience**, v.11, n.7, p. 823-833, 1 jul. 2008. Available at <https://doi.org/10.1038/nn.2134>. Accessed on: 6 dec. 2019.

GEISLER, C. et al. Hippocampal place cell assemblies are speed-controlled oscillators. **Proceedings of the National Academy of Sciences**, v.104, n.19, p. 8149-8154, 8 may. 2007. Available at <https://doi.org/10.1073/pnas.0610121104>. Accessed on: 21 aug. 2019.

GÓIS, Z. H. T.; TORT, A. B. Characterizing Speed Cells in the Rat Hippocampus. **Cell Reports**, v.25, n.7, p. 1872-1884.e4, 1 nov. 2018. Available at <https://doi.org/10.1016/j.celrep.2018.10.054>. Accessed on: 6 dec. 2019.

GONZALEZ, W. G. et al. Persistence of neuronal representations through time and damage in the hippocampus. **Science**, v.365, n.6455, p. 821-825, 23 aug. 2019. Available at <https://doi.org/10.1126/science.aav9199>. Accessed on: 23 aug. 2019.

GRIEVES, R. M.; JEFFERY, K. J. The representation of space in the brain. **Behavioural Processes**, v.135, n.NaN, p. 113-131, 1 feb. 2017. Available at <https://doi.org/10.1016/j.beproc.2016.12.012>. Accessed on: 6 dec. 2019.

HAFTING, T. et al. Microstructure of a spatial map in the entorhinal cortex. **Nature**, v.436, n.7052, p. 801-806, 1 aug. 2005. Available at <https://doi.org/10.1038/nature03721>. Accessed on: 21 aug. 2019.

HAFTING, T. et al. Microstructure of a spatial map in the entorhinal cortex. **Nature**, v.436, n.7052, p. 801-806, 1 aug. 2005. Available at <https://doi.org/10.1038/nature03721>. Accessed on: 19 feb. 2020.

HARDCASTLE, K. et al. A Multiplexed, Heterogeneous, and Adaptive Code for Navigation in Medial Entorhinal Cortex. **Neuron**, v.94, n.2, p. 375-387.e7, 1 apr. 2017. Available at <https://doi.org/10.1016/j.neuron.2017.03.025>. Accessed on: 6 dec. 2019.

HARRIS, K. D. et al. Accuracy of Tetrode Spike Separation as Determined by Simultaneous Intracellular and Extracellular Measurements. **Journal of Neurophysiology**, v.84, n.1, p. 401-414, 1 jul. 2000. Available at <https://doi.org/10.1152/jn.2000.84.1.401>. Accessed on: 21 aug. 2019.

HARTLEY T. et al. Space in the brain: how the hippocampal formation supports spatial cognition. **Philosophical Transactions of the Royal Society B: Biological Sciences**, v.369,

n.1635, p. 20120510, 5 feb. 2014. Available at <https://doi.org/10.1098/rstb.2012.0510>. Accessed on: 21 aug. 2019.

HAZAN, L.; ZUGARO, M.; BUZSÁKI, G. Klusters, NeuroScope, NDManager: A free software suite for neurophysiological data processing and visualization. **Journal of Neuroscience Methods**, v.155, n.2, p. 207-216, 1 sep. 2006. Available at <https://doi.org/10.1016/j.jneumeth.2006.01.017>. Accessed on: 6 dec. 2019.

HINMAN, J. R. et al. Multiple Running Speed Signals in Medial Entorhinal Cortex. **Neuron**, v.91, n.3, p. 666-679, 1 aug. 2016. Available at <https://doi.org/10.1016/j.neuron.2016.06.027>. Accessed on: 6 dec. 2019.

HINMAN, J. R. et al. Septotemporal variation in dynamics of theta: speed and habituation. **Journal of Neurophysiology**, v.105, n.6, p. 2675-2686, 1 jun. 2011. Available at <https://doi.org/10.1152/jn.00837.2010>. Accessed on: 6 dec. 2019.

HIRASE, H. et al. Firing rate and theta-phase coding by hippocampal pyramidal neurons during ‘space clamping’: Theta phase of hippocampal pyramidal cells. **European Journal of Neuroscience**, v.11, n.12, p. 4373-4380, 1 dec. 1999. Available at <https://doi.org/10.1046/j.1460-9568.1999.00853.x>. Accessed on: 6 dec. 2019.

HUXTER, J.; BURGESS, N.; O'KEEFE, J. Independent rate and temporal coding in hippocampal pyramidal cells. **Nature**, v.425, n.6960, p. 828–832, 23 oct. 2003. Available at <https://doi.org/10.1038/nature02058>. Accessed on: 19 feb. 2020.

KLAUSBERGER, T. et al. Brain-state- and cell-type-specific firing of hippocampal interneurons in vivo. **Nature**, v.421, n.6925, p. 844-848, 1 feb. 2003. Available at <https://doi.org/10.1038/nature01374>. Accessed on: 21 aug. 2019.

KLAUSBERGER, T.; SOMOGYI, P. Neuronal Diversity and Temporal Dynamics: The Unity of Hippocampal Circuit Operations. **Science**, v.321, n.5885, p. 53-57, 4 jul. 2008. Available at <https://doi.org/10.1126/science.1149381>. Accessed on: 21 aug. 2019.

KNIERIM, J. J.; KUDRIMOTI, H. S.; MCNAUGHTON, B. L. Interactions between idiothetic cues and external landmarks in the control of place cells and head direction cells.

Journal of Neurophysiology, v.80, n.1, p. 425–446, 1 jul. 1998. Available at <https://doi.org/10.1152/jn.1998.80.1.425>. Accessed on: 19 feb. 2020.

KROPFF, E. et al. Speed cells in the medial entorhinal cortex. **Nature**, v.523, n.7561, p. 419-424, 1 jul. 2015. Available at <https://doi.org/10.1038/nature14622>. Accessed on: 21 aug. 2019.

LEVER, C. et al. Spatial coding in the hippocampal formation: input, information type, plasticity, and behaviour. [s.l.] **Oxford University Press**, 6 nov. 2003. Available at <https://doi.org/10.1093/acprof:oso/9780198515241.003.0011>. Accessed on: 21 aug. 2019.

MAURER, A. P. et al. Self-motion and the origin of differential spatial scaling along the septo-temporal axis of the hippocampus. **Hippocampus**, v.15, n.7, p. 841-852, 1 jan. 2005. Available at <https://doi.org/10.1002/hipo.20114>. Accessed on: 21 aug. 2019.

MCNAUGHTON, B. L. et al. Deciphering the hippocampal polyglot: the hippocampus as a path integration system. **Journal of Experimental Biology**, v.199, n.1, p. 173-185, 1 jan. 1996. Available at <https://jeb.biologists.org/content/199/1/173>. Accessed on: 21 aug. 2019.

MCNAUGHTON, B. L.; BARNES, C. A.; O'KEEFE, J. The contributions of position, direction, and velocity to single unit activity in the hippocampus of freely-moving rats. **Experimental Brain Research**, v.52, n.1, p. 41-49, 1 sep. 1983. Available at <https://doi.org/10.1007/BF00237147>. Accessed on: 21 aug. 2019.

MCNAUGHTON, B. L.; LEONARD, B.; CHEN, L. Cortical-hippocampal interactions and cognitive mapping: A hypothesis based on reintegration of the parietal and inferotemporal pathways for visual processing. **Psychobiology**, v.17, n.3, p. 230-235, 1 sep. 1989. Available at <https://doi.org/10.1007/BF03337774>. Accessed on: 21 aug. 2019.

MCNAUGHTON, B. L. et al. Path integration and the neural basis of the 'cognitive map'. **Nature Reviews Neuroscience**, v.7, n.8, p. 663-678, 1 aug. 2006. Available at <https://doi.org/10.1038/nrn1932>. Accessed on: 21 aug. 2019.

MIZUSEKI, K. et al. Neurosharing: large-scale data sets (spike, LFP) recorded from the hippocampal-entorhinal system in behaving rats. **F1000Research**, v.3, n.NaN, p. 98, 30 apr.

2014. Available at <https://doi.org/10.12688/f1000research.3895.2>. Accessed on: 21 aug. 2019.

MIZUSEKI, K. et al. Theta Oscillations Provide Temporal Windows for Local Circuit Computation in the Entorhinal-Hippocampal Loop. **Neuron**, v.64, n.2, p. 267-280, 1 oct. 2009. Available at <https://doi.org/10.1016/j.neuron.2009.08.037>. Accessed on: 6 dec. 2019.

MOSER, E. I.; KROPFF, E.; MOSER, M. Place Cells, Grid Cells, and the Brain's Spatial Representation System. **Annual Review of Neuroscience**, v.31, n.1, p. 69-89, 1 jul. 2008. Available at <https://doi.org/10.1146/annurev.neuro.31.061307.090723>. Accessed on: 6 dec. 2019.

MULLER, R. U. et al. On the directional firing properties of hippocampal place cells. **The Journal of Neuroscience: The Official Journal of the Society for Neuroscience**, v.14, n.12, p. 7235-7251, 1 dec. 1994. Available at <https://doi.org/10.1523/JNEUROSCI.14-12-07235.1994>. Accessed on: 19 feb. 2020.

MULLER, R. U.; KUBIE, J. L. The effects of changes in the environment on the spatial firing of hippocampal complex-spike cells. **Journal of Neuroscience**, v.7, n.7, p. 1951-1968, 1 jul. 1987. Available at <https://doi.org/10.1523/JNEUROSCI.07-07-01951.1987>. Accessed on: 21 aug. 2019.

NAVRATILOVA, Z. et al. Phase precession and variable spatial scaling in a periodic attractor map model of medial entorhinal grid cells with realistic after-spike dynamics. **Hippocampus**, v.22, n.4, p. 772-789, 1 apr. 2012. Available at <https://doi.org/10.1002/hipo.20939>. Accessed on: 6 dec. 2019.

NITZ, D.; MCNAUGHTON, B. Differential Modulation of CA1 and Dentate Gyrus Interneurons During Exploration of Novel Environments. **Journal of Neurophysiology**, v.91, n.2, p. 863-872, 1 feb. 2004. Available at <https://doi.org/10.1152/jn.00614.2003>. Accessed on: 6 dec. 2019.

O'KEEFE, J. et al. Place cells, navigational accuracy, and the human hippocampus. **Philosophical Transactions of the Royal Society of London**. Series B, Biological Sciences, v.353, n.1373, p. 1333–1340, 29 aug. 1998. Available at <https://doi.org/10.1098/rstb.1998.0287>. Accessed on: 19 feb. 2020.

O'KEEFE, J.; CONWAY, D. Hippocampal place units in the freely moving rat: Why they fire where they fire. **Experimental Brain Research**, v.31, n.4, p. , 1 apr. 1978. Available at <https://doi.org/10.1007/BF00239813>. Accessed on: 6 dec. 2019.

O'KEEFE, J.; DOSTROVSKY, J. The hippocampus as a spatial map. Preliminary evidence from unit activity in the freely-moving rat. **Brain Research**, v.34, n.1, p. 171-175, 1 nov. 1971. Available at <https://doi.org/10.1016/0006-8993(71)90358-1>. Accessed on: 6 dec. 2019.

O'KEEFE, J.; SPEAKMAN, A. Single unit activity in the rat hippocampus during a spatial memory task. **Experimental Brain Research**, v.68, n.1, p. 1-27, 1 sep. 1987. Available at <https://doi.org/10.1007/BF00255230>. Accessed on: 21 aug. 2019.

O'KEEFE, J. Place units in the hippocampus of the freely moving rat. **Experimental Neurology**, v.51, n.1, p. 78-109, 1 jan. 1976. Available at <https://doi.org/10.1016/0014-4886(76)90055-8>. Accessed on: 21 aug. 2019.

PARK, S. H. et al. History of Bioelectrical Study and the Electrophysiology of the Primo Vascular System. **Evidence-Based Complementary and Alternative Medicine**, v.2013, p. 1-14, 1 jan. 2013. Available at <https://doi.org/10.1155/2013/486823>. Accessed on: 24 sep. 2019.

PELKEY, K. A. et al. Hippocampal GABAergic Inhibitory Interneurons. **Physiological Reviews**, v.97, n.4, p. 1619-1747, 1 oct. 2017. Available at <https://doi.org/10.1152/physrev.00007.2017>. Accessed on: 6 dec. 2019.

PÉREZ-ESCOBAR, J. A. et al. Visual landmarks sharpen grid cell metric and confer context specificity to neurons of the medial entorhinal cortex. **eLife**, v.5, p. e16937, 23 jul. 2016. Available at <https://doi.org/10.7554/eLife.16937>. Accessed on: 21 aug. 2019.

PRESS, T. M. Spikes. **The MIT Press**, 1 jun. 1999. Available at <https://mitpress.mit.edu/books/spikes>. Accessed on: 21 aug. 2019.

QUIAN Q. R.; PANZERI, S. Extracting information from neuronal populations: information theory and decoding approaches. **Nature Reviews Neuroscience**, v.10, n.3, p. 173-185, 1 mar. 2009. Available at <https://doi.org/10.1038/nrn2578>. Accessed on: 6 dec. 2019.

QUIRK, G. J.; MULLER, R. U.; KUBIE, J. L. The firing of hippocampal place cells in the dark depends on the rat's recent experience. **Journal of Neuroscience**, v.10, n.6, p. 2008-2017, 1 jun. 1990. Available at <https://doi.org/10.1523/JNEUROSCI.10-06-02008.1990>. Accessed on: 21 aug. 2019.

ROLLS, E. T.; TREVES, A. The neuronal encoding of information in the brain. **Progress in Neurobiology**, v.95, n.3, p. 448-490, 1 nov. 2011. Available at <https://doi.org/10.1016/j.pneurobio.2011.08.002>. Accessed on: 21 aug. 2019.

SANDERS, H. et al. Grid Cells and Place Cells: An Integrated View of their Navigational and Memory Function. **Trends in Neurosciences**, v.38, n.12, p. 763-775, 1 dec. 2015. Available at <https://doi.org/10.1016/j.tins.2015.10.004>. Accessed on: 21 aug. 2019.

SARGOLINI, F. et al. Conjunctive Representation of Position, Direction, and Velocity in Entorhinal Cortex. **Science**, v.312, n.5774, p. 758-762, 5 may. 2006. Available at <https://doi.org/10.1126/science.1125572>. Accessed on: 21 aug. 2019.

SHARP, P. E.; TURNER-WILLIAMS, S. Movement-Related Correlates of Single-Cell Activity in the Medial Mammillary Nucleus of the Rat During a Pellet-Chasing Task. **Journal of Neurophysiology**, v.94, n.3, p. 1920-1927, 1 sep. 2005. Available at <https://doi.org/10.1152/jn.00194.2005>. Accessed on: 19 feb. 2020.

SHARP, P. E.; TURNER-WILLIAMS, S.; TUTTLE, S. Movement-related correlates of single cell activity in the interpeduncular nucleus and habenula of the rat during a pellet-chasing task. **Behavioural Brain Research**, v.166, n.1, p. 55-70, 1 jan. 2006. Available at <https://doi.org/10.1016/j.bbr.2005.07.004>. Accessed on: 14 feb. 2020.

SHARP, P.; KUBIE, J.; MULLER, R. Firing properties of hippocampal neurons in a visually symmetrical environment: contributions of multiple sensory cues and mnemonic processes. **The Journal of Neuroscience**, v.10, n.9, p. 3093-3105, 1 sep. 1990. Available at <https://doi.org/10.1523/JNEUROSCI.10-09-03093.1990>. Accessed on: 21 aug. 2019.

SHEERAN, W. M.; AHMED, O. J. The Neural Circuitry Supporting Successful Spatial Navigation despite Variable Movement Speeds. **Neuroscience & Biobehavioral Reviews** , 21 nov. 2019. Available at <https://doi.org/10.1016/j.neubiorev.2019.11.013>. Accessed on: 6 dec. 2019.

SIROTA, A. et al. Entrainment of neocortical neurons and gamma oscillations by the hippocampal theta rhythm. **Neuron**, v.60, n.4, p. 683–697, 26 nov. 2008. Available at <https://doi.org/10.1016/j.neuron.2008.09.014>. Accessed on: 19 feb. 2020.

SŁAWIŃSKA, U.; KASICKI, S. The frequency of rat's hippocampal theta rhythm is related to the speed of locomotion. **Brain Research**, v.796, n.1, p. 327-331, 15 jun. 1998. Available at <https://doi.org/10.1016/S0006-8993(98)00390-4>. Accessed on: 21 aug. 2019.

STANLEY, G. B. Reading and writing the neural code. **Nature Neuroscience**, v.16, n.3, p. 259-263, 1 mar. 2013. Available at <https://doi.org/10.1038/nn.3330>. Accessed on: 21 aug. 2019.

TAUBE, J.; MULLER, R.; RANCK, J. Head-direction cells recorded from the postsubiculum in freely moving rats. I. Description and quantitative analysis. **The Journal of Neuroscience**, v.10, n.2, p. 420-435, 1 feb. 1990. Available at <https://doi.org/10.1523/JNEUROSCI.10-02-00420.1990>. Accessed on: 19 feb. 2020.

TAUBE, J.; MULLER, R.; RANCK, J. Head-direction cells recorded from the postsubiculum in freely moving rats. II. Effects of environmental manipulations. **The Journal of Neuroscience**, v.10, n.2, p. 436-447, 1 feb. 1990. Available at <https://doi.org/10.1523/JNEUROSCI.10-02-00436.1990>. Accessed on: 19 feb. 2020.

WHISHAW, I. Q. Place Learning in Hippocampal Rats and the Path Integration Hypothesis. **Neuroscience & Biobehavioral Reviews**, v.22, n.2, p. 209-220, 1 mar. 1998. Available at <https://doi.org/10.1016/S0149-7634(97)00002-X>. Accessed on: 21 aug. 2019.

WHISHAW, I. Q.; BROOKS, B. L. Calibrating space: Exploration is important for allothetic and idiothetic navigation. **Hippocampus**, v.9, n.6, p. 659-667, 1 jan. 1999. Available at <https://doi.org/10.1002/(SICI)1098-1063(1999)9:6%3C659::AID-HIPO7%3E3.0.CO;2-E>. Accessed on: 21 aug. 2019.

WILLS, T. J.; BARRY, C.; CACUCCI, F. The abrupt development of adult-like grid cell firing in the medial entorhinal cortex. **Frontiers in Neural Circuits**, v.6, n.NaN, p. , 1 jan. 2012. Available at <https://doi.org/10.3389/fncir.2012.00021>. Accessed on: 6 dec. 2019.

WILLS, T. J. et al. Development of the Hippocampal Cognitive Map in Preweanling Rats. **Science**, v.328, n.5985, p. 1573-1576, 18 jun. 2010. Available at <https://doi.org/10.1126/science.1188224>. Accessed on: 23 aug. 2019.

WOOD, E. R. et al. Hippocampal Neurons Encode Information about Different Types of Memory Episodes Occurring in the Same Location. **Neuron**, v.27, n.3, p. 623-633, 1 sep. 2000. Available at <https://doi.org/10.1016/S0896-6273(00)00071-4>. Accessed on: 21 aug. 2019.

YE, J. et al. Entorhinal fast-spiking speed cells project to the hippocampus. **Proceedings of the National Academy of Sciences**, v.115, n.7, p. E1627-E1636, 13 feb. 2018. Available at <https://doi.org/10.1073/pnas.1720855115>. Accessed on: 6 dec. 2019.

ZHANG, K. et al. Interpreting neuronal population activity by Reconstruction: Unified Framework With Application to Hippocampal Place Cells. **Journal of Neurophysiology**, v.79, n.2, p. 1017-1044, 1 feb. 1998. Available at <https://doi.org/10.1152/jn.1998.79.2.1017>. Accessed on: 6 dec. 2019.

ARONOV, D.; NEVERS, R.; TANK, D. W. Mapping of a Non-Spatial Dimension by the Hippocampal–Entorhinal Circuit. **Nature**, v. 543, n. 7647, p. 719–722, mar. 2017.

ARRIAGA, M.; HAN, E. B. Dedicated Hippocampal Inhibitory Networks for Locomotion and Immobility. **Journal of Neuroscience**, v. 37, n. 38, p. 9222–9238, 20 set. 2017.

BIALEK, W. et al. Reading a Neural Code. **Science**, v. 252, n. 5014, p. 1854–1857, 28 jun. 1991.

BUCKNER, R. L. The Role of the Hippocampus in Prediction and Imagination. **Annual Review of Psychology**, v. 61, n. 1, p. 27–48, jan. 2010.

BURAK, Y.; FIETE, I. R. Accurate Path Integration in Continuous Attractor Network Models of Grid Cells. **PLOS Computational Biology**, v. 5, n. 2, p. e1000291, 20 fev. 2009.

BUZSÁKI, G. Theta Oscillations in the Hippocampus. **Neuron**, v. 33, n. 3, p. 325–340, 31 jan. 2002.

BUZSÁKI, G. Theta Rhythm of Navigation: Link between Path Integration and Landmark Navigation, Episodic and Semantic Memory. **Hippocampus**, v. 15, n. 7, p. 827–840, 2005.

BUZSÁKI, G. Neural Syntax: Cell Assemblies, Synapsembles, and Readers. **Neuron**, v. 68, n. 3, p. 362–385, 4 nov. 2010.

BUZSÁKI, G.; MOSER, E. I. Memory, Navigation and Theta Rhythm in the Hippocampal-Entorhinal System. **Nature Neuroscience**, v. 16, n. 2, p. 130–138, fev. 2013.

CHADWICK, A.; VAN ROSSUM, M. C.; NOLAN, M. F. Flexible Theta Sequence Compression Mediated via Phase Precessing Interneurons. **eLife**, v. 5, p. e20349, 8 dez. 2016.

COUEY, J. J. et al. Recurrent Inhibitory Circuitry as a Mechanism for Grid Formation. **Nature Neuroscience**, v. 16, n. 3, p. 318–324, mar. 2013.

CSICSVARI, J. et al. Oscillatory Coupling of Hippocampal Pyramidal Cells and Interneurons in the Behaving Rat. **Journal of Neuroscience**, v. 19, n. 1, p. 274–287, 1 jan. 1999.

CZURKÓ, A. et al. Sustained Activation of Hippocampal Pyramidal Cells by ‘Space Clamping’ in a Running Wheel: Sustained Discharge of Hippocampal Pyramidal Cells. **European Journal of Neuroscience**, v. 11, n. 1, p. 344–352, jan. 1999.

CZURKÓ, A. et al. Theta Phase Classification of Interneurons in the Hippocampal Formation of Freely Moving Rats. **Journal of Neuroscience**, v. 31, n. 8, p. 2938–2947, 23 fev. 2011.

DIBA, K.; BUZSÁKI, G. Hippocampal Network Dynamics Constrain the Time Lag between Pyramidal Cells across Modified Environments. **Journal of Neuroscience**, v. 28, n. 50, p. 13448–13456, 10 dez. 2008.

DRAGOI, G.; BUZSÁKI, G. Temporal Encoding of Place Sequences by Hippocampal Cell Assemblies. **Neuron**, v. 50, n. 1, p. 145–157, abr. 2006.

EICHENBAUM, H. Hippocampus: Mapping or memory? **Current Biology**, v. 10, n. 21, p. R785–R787, 1 nov. 2000.

EKSTROM, A. D. et al. NMDA Receptor Antagonism Blocks Experience-Dependent Expansion of Hippocampal “Place Fields”. **Neuron**, v. 31, n. 4, p. 631–638, ago. 2001.

FERBINTEANU, J.; SHAPIRO, M. L. Prospective and Retrospective Memory Coding in the Hippocampus. **Neuron**, v. 40, n. 6, p. 1227–1239, dez. 2003.

FRANK, L. M.; BROWN, E. N.; WILSON, M. A. A Comparison of the Firing Properties of Putative Excitatory and Inhibitory Neurons From CA1 and the Entorhinal Cortex. **Journal of Neurophysiology**, v. 86, n. 4, p. 2029–2040, 1 out. 2001.

FREUND, T. f.; BUZSÁKI, G. Interneurons of the hippocampus. **Hippocampus**, v. 6, n. 4, p. 347–470, 1 jan. 1996.

FUHRMANN, F. et al. Locomotion, Theta Oscillations, and the Speed-Correlated Firing of Hippocampal Neurons Are Controlled by a Medial Septal Glutamatergic Circuit. **Neuron**, v. 86, n. 5, p. 1253–1264, jun. 2015.

FUHS, M. C.; TOURETZKY, D. S. A Spin Glass Model of Path Integration in Rat Medial Entorhinal Cortex. **Journal of Neuroscience**, v. 26, n. 16, p. 4266–4276, 19 abr. 2006.

FUJISAWA, S. et al. Behavior-Dependent Short-Term Assembly Dynamics in the Medial Prefrontal Cortex. **Nature Neuroscience**, v. 11, n. 7, p. 823–833, jul. 2008.

GEISLER, C. et al. Hippocampal Place Cell Assemblies Are Speed-Controlled Oscillators. **Proceedings of the National Academy of Sciences**, v. 104, n. 19, p. 8149–8154, 8 maio 2007.

HAFTING, T. et al. Microstructure of a Spatial Map in the Entorhinal Cortex. **Nature**, v. 436, n. 7052, p. 801–806, ago. 2005.

HARDCASTLE, K. et al. A Multiplexed, Heterogeneous, and Adaptive Code for Navigation in Medial Entorhinal Cortex. **Neuron**, v. 94, n. 2, p. 375- 387.e7, abr. 2017.

HARRIS, K. D. et al. Accuracy of Tetrode Spike Separation as Determined by Simultaneous Intracellular and Extracellular Measurements. **Journal of Neurophysiology**, v. 84, n. 1, p. 401–414, 1 jul. 2000.

HARTLEY TOM et al. Space in the brain: how the hippocampal formation supports spatial cognition. **Philosophical Transactions of the Royal Society B: Biological Sciences**, v. 369, n. 1635, p. 20120510, 5 fev. 2014.

HAZAN, L.; ZUGARO, M.; BUZSÁKI, G. Klusters, NeuroScope, NDManager: A Free Software Suite for Neurophysiological Data Processing and Visualization. **Journal of Neuroscience Methods**, v. 155, n. 2, p. 207–216, set. 2006.

HINMAN, J. R. et al. Septotemporal Variation in Dynamics of Theta: Speed and Habituation. **Journal of Neurophysiology**, v. 105, n. 6, p. 2675–2686, jun. 2011.

HINMAN, J. R. et al. Multiple Running Speed Signals in Medial Entorhinal Cortex. **Neuron**, v. 91, n. 3, p. 666–679, ago. 2016.

HIRASE, H. et al. Firing Rate and Theta-Phase Coding by Hippocampal Pyramidal Neurons during 'Space Clamping': Theta Phase of Hippocampal Pyramidal Cells. **European Journal of Neuroscience**, v. 11, n. 12, p. 4373–4380, dez. 1999.

HUXTER, J.; BURGESS, N.; O'KEEFE, J. Independent rate and temporal coding in hippocampal pyramidal cells. **Nature**, v. 425, n. 6960, p. 828–832, 23 out. 2003.

KLAUSBERGER, T. et al. Brain-State- and Cell-Type-Specific Firing of Hippocampal Interneurons in Vivo. **Nature**, v. 421, n. 6925, p. 844–848, fev. 2003.

KLAUSBERGER, T.; SOMOGYI, P. Neuronal Diversity and Temporal Dynamics: The Unity of Hippocampal Circuit Operations. **Science**, v. 321, n. 5885, p. 53–57, 4 jul. 2008.

KNIERIM, J. J.; KUDRIMOTI, H. S.; MCNAUGHTON, B. L. Interactions between idiothetic cues and external landmarks in the control of place cells and head direction cells. **Journal of Neurophysiology**, v. 80, n. 1, p. 425–446, jul. 1998.

KROPFF, E. et al. Speed Cells in the Medial Entorhinal Cortex. **Nature**, v. 523, n. 7561, p. 419–424, jul. 2015.

LEVER, C. et al. **Spatial coding in the hippocampal formation: input, information type, plasticity, and behaviour**. [s.l.] Oxford University Press, 2003.

MAURER, A. P. et al. Self-Motion and the Origin of Differential Spatial Scaling along the Septo-Temporal Axis of the Hippocampus. **Hippocampus**, v. 15, n. 7, p. 841–852, 2005.

MCNAUGHTON, B. L. et al. Deciphering the Hippocampal Polyglot: The Hippocampus as a Path Integration System. **Journal of Experimental Biology**, v. 199, n. 1, p. 173–185, 1 jan. 1996.

MCNAUGHTON, B. L. et al. Path Integration and the Neural Basis of the "Cognitive Map". **Nature Reviews Neuroscience**, v. 7, n. 8, p. 663–678, ago. 2006.

MCNAUGHTON, B. L.; BARNES, C. A.; O'KEEFE, J. The Contributions of Position, Direction, and Velocity to Single Unit Activity in the Hippocampus of Freely-Moving Rats. **Experimental Brain Research**, v. 52, n. 1, p. 41–49, 1 set. 1983.

MIZUSEKI, K. et al. Theta Oscillations Provide Temporal Windows for Local Circuit Computation in the Entorhinal-Hippocampal Loop. **Neuron**, v. 64, n. 2, p. 267–280, out. 2009.

MIZUSEKI, K. et al. Multiple single unit recordings from different rat hippocampal and entorhinal regions while the animals were performing multiple behavioral tasks. **CRCNS org**, 2013.

MIZUSEKI, K. et al. Neurosharing: Large-Scale Data Sets (Spike, LFP) Recorded from the Hippocampal-Entorhinal System in Behaving Rats. **F1000Research**, v. 3, p. 98, 30 abr. 2014.

MOSER, E. I.; KROPFF, E.; MOSER, M.-B. Place Cells, Grid Cells, and the Brain's Spatial Representation System. **Annual Review of Neuroscience**, v. 31, n. 1, p. 69–89, jul. 2008.

MULLER, R. U. et al. On the Directional Firing Properties of Hippocampal Place Cells. **The Journal of Neuroscience: The Official Journal of the Society for Neuroscience**, v. 14, n. 12, p. 7235–7251, dez. 1994.

MULLER, R. U.; KUBIE, J. L. The Effects of Changes in the Environment on the Spatial Firing of Hippocampal Complex-Spike Cells. **Journal of Neuroscience**, v. 7, n. 7, p. 1951–1968, 1 jul. 1987.

NAVRATILOVA, Z. et al. Phase Precession and Variable Spatial Scaling in a Periodic Attractor Map Model of Medial Entorhinal Grid Cells with Realistic After-Spike Dynamics. **Hippocampus**, v. 22, n. 4, p. 772–789, abr. 2012.

NITZ, D.; MCNAUGHTON, B. Differential Modulation of CA1 and Dentate Gyrus Interneurons During Exploration of Novel Environments. **Journal of Neurophysiology**, v. 91, n. 2, p. 863–872, fev. 2004.

O'KEEFE, J. Place units in the hippocampus of the freely moving rat. **Experimental Neurology**, v. 51, n. 1, p. 78–109, 1 jan. 1976.

O'KEEFE, J. et al. Place cells, navigational accuracy, and the human hippocampus. **Philosophical Transactions of the Royal Society of London. Series B, Biological Sciences**, v. 353, n. 1373, p. 1333–1340, 29 ago. 1998.

O'KEEFE, J.; CONWAY, D. H. Hippocampal Place Units in the Freely Moving Rat: Why They Fire Where They Fire. **Experimental Brain Research**, v. 31, n. 4, abr. 1978. Disponível em: <https://doi.org/10.1007/BF00239813>. Acesso em: 6 dez. 2019.

O'KEEFE, J.; DOSTROVSKY, J. The Hippocampus as a Spatial Map. Preliminary Evidence from Unit Activity in the Freely-Moving Rat. **Brain Research**, v. 34, n. 1, p. 171–175, nov. 1971.

O'KEEFE, J.; SPEAKMAN, A. Single Unit Activity in the Rat Hippocampus during a Spatial Memory Task. **Experimental Brain Research**, v. 68, n. 1, p. 1–27, 1 set. 1987.

PELKEY, K. A. et al. Hippocampal GABAergic Inhibitory Interneurons. **Physiological Reviews**, v. 97, n. 4, p. 1619–1747, 1 out. 2017.

PÉREZ-ESCOBAR, J. A. et al. Visual Landmarks Sharpen Grid Cell Metric and Confer Context Specificity to Neurons of the Medial Entorhinal Cortex. **eLife**, v. 5, p. e16937, 23 jul. 2016.

QUIAN QUIROGA, R.; PANZERI, S. Extracting Information from Neuronal Populations: Information Theory and Decoding Approaches. **Nature Reviews Neuroscience**, v. 10, n. 3, p. 173–185, mar. 2009.

RIEKE, F. **Spikes: exploring the neural code**. [s.l.] MIT press, 1999.

ROLLS, E. T.; TREVES, A. The neuronal encoding of information in the brain. **Progress in Neurobiology**, v. 95, n. 3, p. 448–490, 1 nov. 2011.

SANDERS, H. et al. Grid Cells and Place Cells: An Integrated View of their Navigational and Memory Function. **Trends in Neurosciences**, v. 38, n. 12, p. 763–775, 1 dez. 2015.

SARGOLINI, F. et al. Conjunctive Representation of Position, Direction, and Velocity in Entorhinal Cortex. **Science**, v. 312, n. 5774, p. 758–762, 5 maio 2006.

SHARP, P. E.; TURNER-WILLIAMS, S. Movement-Related Correlates of Single-Cell Activity in the Medial Mammillary Nucleus of the Rat During a Pellet-Chasing Task. **Journal of Neurophysiology**, v. 94, n. 3, p. 1920–1927, set. 2005.

SHARP, P. E.; TURNER-WILLIAMS, S.; TUTTLE, S. Movement-Related Correlates of Single Cell Activity in the Interpeduncular Nucleus and Habenula of the Rat during a Pellet-Chasing Task. **Behavioural Brain Research**, v. 166, n. 1, p. 55–70, jan. 2006.

SHARP, P.; KUBIE, J.; MULLER, R. Firing Properties of Hippocampal Neurons in a Visually Symmetrical Environment: Contributions of Multiple Sensory Cues and Mnemonic Processes. **The Journal of Neuroscience**, v. 10, n. 9, p. 3093–3105, 1 set. 1990.

SIROTA, A. et al. Entrainment of neocortical neurons and gamma oscillations by the hippocampal theta rhythm. **Neuron**, v. 60, n. 4, p. 683–697, 26 nov. 2008.

SŁAWIŃSKA, U.; KASICKI, S. The frequency of rat's hippocampal theta rhythm is related to the speed of locomotion. **Brain Research**, v. 796, n. 1, p. 327–331, 15 jun. 1998.

STANLEY, G. B. Reading and Writing the Neural Code. **Nature Neuroscience**, v. 16, n. 3, p. 259–263, mar. 2013.

TAUBE, J.; MULLER, R.; RANCK, J. Head-Direction Cells Recorded from the Postsubiculum in Freely Moving Rats. I. Description and Quantitative Analysis. **The Journal of Neuroscience**, v. 10, n. 2, p. 420–435, 1 fev. 1990.

WHISHAW, I. Q. Place Learning in Hippocampal Rats and the Path Integration Hypothesis. **Neuroscience & Biobehavioral Reviews**, v. 22, n. 2, p. 209–220, 1 mar. 1998.

WHISHAW, I. Q.; BROOKS, B. L. Calibrating Space: Exploration Is Important for Allothetic and Idiothetic Navigation. **Hippocampus**, v. 9, n. 6, p. 659–667, 1999.

WIENER, S. I.; PAUL, C. A.; EICHENBAUM, H. Spatial and behavioral correlates of hippocampal neuronal activity. **The Journal of Neuroscience**, v. 9, n. 8, p. 2737–2763, ago. 1989.

WILLS, T. J.; BARRY, C.; CACUCCI, F. The Abrupt Development of Adult-like Grid Cell Firing in the Medial Entorhinal Cortex. **Frontiers in Neural Circuits**, v. 6, 2012. Disponível em: <https://doi.org/10.3389/fncir.2012.00021>. Acesso em: 6 dez. 2019.

WOOD, E. R. et al. Hippocampal Neurons Encode Information about Different Types of Memory Episodes Occurring in the Same Location. **Neuron**, v. 27, n. 3, p. 623–633, 1 set. 2000.

YE, J. et al. Entorhinal Fast-Spiking Speed Cells Project to the Hippocampus. **Proceedings of the National Academy of Sciences**, v. 115, n. 7, p. E1627–E1636, 13 fev. 2018.

ZHANG, K. et al. Interpreting Neuronal Population Activity by Reconstruction: Unified Framework With Application to Hippocampal Place Cells. **Journal of Neurophysiology**, v. 79, n. 2, p. 1017–1044, 1 fev. 1998.

# APENDIX

## APÊNDICE A GRAPHICAL ABSTRACT OF THE PUBLISHED ARTICLE

Article

Cell Reports

### Characterizing Speed Cells in the Rat Hippocampus

#### Graphical Abstract

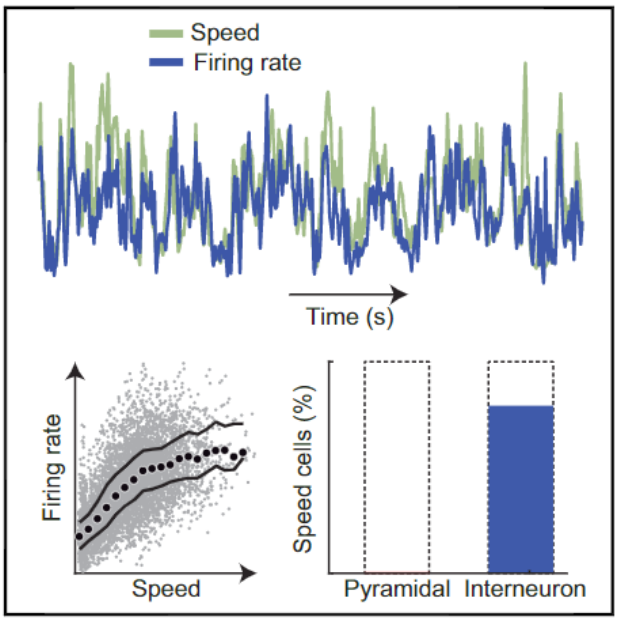


#### Authors

Zé Henrique T.D. Góis, Adriano B.L. Tort

#### Correspondence

tort@neuro.ufrn.br

#### In Brief

Neurons coding for locomotion speed are theoretically required to perform path integration. Góis and Tort show that in CA1, speed is encoded by inhibitory interneurons, but not pyramidal cells, shedding light on the network mechanisms of spatial navigation.

#### Highlights

- The firing rate of a subset of CA1 neurons highly correlates with speed
- The rate coding of CA1 speed cells is stable across space, time, and context
- CA1 speed cells are inhibitory interneurons
- Pyramidal cells are modulated by but do not encode speed on a sub-second timescale

Góis & Tort, 2018, Cell Reports 25, 1872–1884
November 13, 2018 © 2018 The Authors.
https://doi.org/10.1016/j.celrep.2018.10.054

CellPress